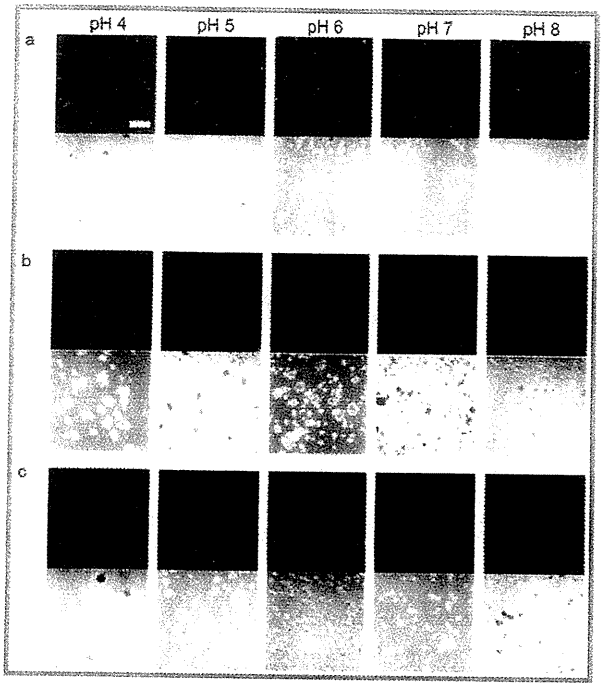

Figure 3. Confocal microscope images of BAps binding to hydroxyapatite in McIlvaine's citrate-phosphate buffer. Scale bar: 40 μm. (a) BAp-A. (b) BAp-M. (c) BAp-E.

Henderson–Hasselbalch equation (Figure 2c). Consequently, the pK_a values of BAp-M and BAp-E were 4.5 and 6.2, respectively. These results indicate that the two pH-activatable probes could be used to selectively visualize the bone-resorbing osteoclasts. On the other hand, BAp-A showed intense fluorescence regardless of pH changes as would be expected by an "always-ON" fluorescence probe.

Hydroxyapatite Binding Test. Bone tissues are mainly composed of type I collagen and hydroxyapatite (HA). Confocal microscopy was then performed to ascertain the HA binding activity and the fluorescence properties of BAps bound to HA. Intense fluorescence was observed from every HA particle, which was mixed with BAp-A and soaked in buffer at different pH values (Figure 3). We next examined the pH-activatable probes, namely, BAp-M and BAp-E. In the case of BAp-M, the fluorescence signals from HA particles were hardly observed under physiological conditions, i.e., at pH 7.0 and pH 8.0. The fluorescence intensities gradually increased with the decrease in the pH value, and consequently, intense fluorescence was observed below pH 5.0. Similar to the behavior in solution, the HA particle including BAp-E responded in an environment of higher pH relative to BAp-M, and showed intense fluorescence. However, the fluorescence signals were very weak or not observed at pH 7.0 or 8.0. These results indicate that BAps are pH-sensitive not only in aqueous solution but also in the solid state, when bound to HA. It was thus expected that synthesized probes could be immobilized on bone tissue and that they will retain their pH-sensitive properties in vivo.

In Vivo Imaging of Osteoclasts. To clarify the osteoclast function and develop new therapeutic agents to treat bone diseases, real-time monitoring of living osteoclasts in vivo will be very important. However, it is challenging to observe living osteoclasts that are present in the medullary cavity, deep inside the bone.

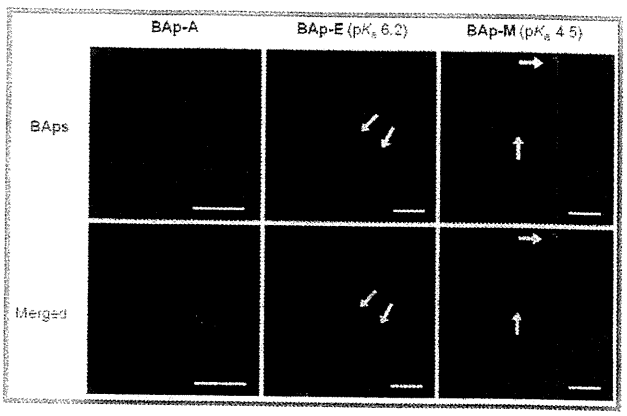

Figure 4. Two-photon excitation microscopy images of in vivo osteoclasts using BAps. PBS solution of BAps (green) was subcutaneously administered daily for 3 days to TRAP-tdTomato (red) transgenic mice. Second harmonic generation from collagen in the bone matrix is presented as a blue signal. Scale bars: 40 μm.

We used two-photon excitation microscopy, which can penetrate deeply into tissues, to capture images of osteoclasts through the parietal bone of mice.[6] The parietal bone is relatively thin, and the distance between the bone surface and the medullary cavity is 80–120 μm. This allowed us to achieve real-time imaging of the active osteoclasts in vivo. To ensure that BAps can function in a living mouse, we administered the probes to mice and evaluated their pH-sensitive properties by the above-described method (Figure 4). The blue signal indicates second harmonic generation from collagen fibers in the bone matrix. It is obvious that osteoclasts were present in the medullary cavity, because we used TRAP (tartrate-resistant acid phosphatase)-tdTomato transgenic mice, in which TRAP-positive mature osteoclasts predominantly express tdTomato.[13] To confirm whether the synthesized probes can be transported and immobilized on the bone tissues, we first used the "always-ON" probe BAp-A (Figure 4). As expected, green fluorescence was observed all over the bone surface. We next examined in vivo imaging of osteoclasts by using pH-activatable probes. In contrast to the case of BAp-A, green signals were locally observed only between the osteoclasts and the bone tissues (Figure 4, white arrow). Although the green staining was also observed in the lower left of the BAp-E panels, it is mainly derived from second harmonic generation from the bone matrix (Figure S2, Supporting Information). These results indicate that our probes are functioning properly, and have the potential to detect the bone-resorbing osteoclasts in vivo. Moreover, it is expected that the pH value in the resorption pit created by an osteoclast should be within the range of 4–6, because more intense fluorescence is found using BAp-E, which has a higher pK_a value relative to BAp-M. The brightness of BAp-E ($\varepsilon_{abs,450} \times \Phi$) between pH 4 and pH 6 is roughly 1.2–7.5 times as intense as that of BAp-M. Until now, the pH value in the resorption pit had not been measured in vivo. Therefore, we expect that this method will be helpful to estimate the pH value in the resorption pits.

CONCLUSION

We demonstrated that our custom-designed probes, in particular, BAp-E, fluoresce in the low-pH environment created by osteoclasts in vivo, as well as in a cuvette. From medicinal and

dx.doi.org/10.1021/ja2064582 |J. Am. Chem. Soc. 2011, 133, 17772–17776

therapeutic points of view, an imaging technique for visualizing the migration and function of osteoclasts is highly desirable. Because this method is the first example of in vivo imaging of a low-pH region created by bone-resorbing osteoclasts, we are confident that the pH-activatable probes BAps will provide a powerful tool for the selective detection of bone-resorbing osteoclasts in vivo.

EXPERIMENTAL SECTION

Synthesis of BAp-A. To a solution of the corresponding bis-carboxylic acid (1,3,5,7-tetramethyl-2,6-bis(2-carboxyethyl)-8-phenyl-4,4-difluoro-4-bora-3a,4a-diaza-*s*-indacene)[11] (9.40 mg, 20.1 μmol) in MeCN (5 mL) were added alendronic acid (5.00 mg, 20.1 μmol) in water (4 mL), 2 N aq NaOH (60 μL, 120 μmol), and DMT-MM (27.7 mg, 100 μmol) at room temperature. After being stirred for 16 h, the reaction mixture was poured into 10% aqueous solution of AcOH (11 mL) and lyophilized. The crude compound was then purified by reverse-phase HPLC under the following conditions: A/B = 85/15 (0 min) to 10/90 (30 min) (solvent A: 100 mM aq TEAA; solvent B: acetonitrile). Compound eluted with a retention time of 12 min was collected. After lyophilization, a orange powder of BAp-A·3Et$_3$N was obtained (6.55 mg, 6.53 μmol) in 32% yield. ^{1}H NMR (400 MHz, D$_2$O) δ 0.95 (s, 3H), 0.97 (s, 3H), 1.12 (t, J = 7.2 Hz, 27H), 1.64–1.67 (m, 2H), 1.75–1.85 (m, 2H), 2.01–2.09 (m, 4H), 2.25–2.37 (m, 10H), 3.00–3.07 (m, 20H), 6.71 (br s, 2H), 7.14 (br s, 3H). HRMS (FAB–) Calcd for [M – H$^+$]$^-$ 698.2021, found 698.2010.

Synthesis of BAp-M. BAp-M was synthesized from the corresponding bis-carboxylic acid (1,3,5,7-tetramethyl-2,6-bis(2-carboxyethyl)-8-(*p*-dimethylaminophenyl-4,4-difluoro-4-bora-3a,4a-diaza-*s*-indacene)[11] by the same method as described above and purified by reverse-phase HPLC under the following conditions: A/B = 75/25 (0 min) to 60/40 (20 min), and then 10/90 (25 min) (solvent A: 100 mM aq TEAA; solvent B: acetonitrile). A orange powder of BAp-M·3Et$_3$N (t_R = 11 min) was obtained in 9% yield. ^{1}H NMR (400 MHz, D$_2$O) δ 1.10–1.14 (m, 33H), 1.63 (br s, 2H), 1.78 (br s, 2H), 2.02–2.10 (m, 4H), 2.28 (s, 3H), 2.32 (s, 3H), 2.41 (br s, 4H), 2.74 (s, 6H), 2.97–3.06 (m, 20H), 6.71 (br s, 4H). HRMS (FAB–) Calcd for [M – H$^+$]$^-$ 741.2443, found 741.2462.

Synthesis of BAp-E. BAp-E was synthesized from the corresponding bis-carboxylic acid (1,3,5,7-tetramethyl-2,6-bis(2-carboxyethyl)-8-(*p*-diethylaminophenyl-4,4-difluoro-4-bora-3a,4a-diaza-*s*-indacene)[11] by the same method as described above and purified by reverse-phase HPLC under the following conditions: A/B = 80/20 (0 min) to 10/90 (30 min) (solvent A: 100 mM aq TEAA; solvent B: acetonitrile). A orange powder of BAp-E·3Et$_3$N (t_R = 13 min) was obtained in 11% yield. ^{1}H NMR (400 MHz, D$_2$O) δ 0.95 (t, J = 7.2 Hz, 6H), 1.08 (s, 3H), 1.13 (t, J = 7.2 Hz, 27H), 1.18 (s, 3H), 1.60–1.65 (m, 2H), 1.71–1.83 (m, 2H), 2.03–2.11 (m, 4H), 2.28 (s, 3H), 2.35 (s, 3H), 2.40–2.46 (m, 4H), 2.93–2.98 (m, 2H), 3.05 (q, J = 7.2 Hz, 18H), 3.34 (q, J = 7.2 Hz, 4H), 6.93 (d, J = 8.0 Hz, 2H), 7.07 (d, J = 8.4 Hz, 2H). HRMS (FAB–) Calcd for [M – H$^+$]$^-$ 769.2756, found 769.2743.

High-Performance Liquid Chromatography. We performed HPLC on a system composed of a pump (PU-2080, JASCO) and a detector (MD-2010, JASCO) with an Inertsil ODS-3 (4.6 mm × 250 mm for analysis; 10.0 mm × 250 mm for preparation).

Fluorometry. Fluorescence spectra were measured in McIlvaine's citrate-phosphate buffer using a Hitachi F4500 spectrometer. Slit width was 2.5 nm for both excitation and emission, and the photomultiplier voltage was 950 V. Fluorescence quantum yields were determined using fluorescein in 0.1 N NaOH as a standard (Φ = 0.85, λ_{ex} = 492 nm).

In Vitro Hydroxyapatite Binding Test. Five milligrams/mL of hydroxyapatite was vortexed in a 1 μM aqueous solution of BAps (1 mL) for 30 min at room temperature. The mixture was centrifuged and washed four times with water. A portion of the residual powder was soaked in citrate-phosphate buffer (400 μL) at various pH values in a glass-bottom dish. Fluorescence images were then collected using a confocal laser scanning microscope (Olympus, FLUOVIEW FV10i) equipped with a 60× lens. The excitation wavelength was 473 nm, and the emission was filtered with a BA490–590 filter.

Two-Photon Excitation Imaging in Mice. The generation of TRAP promoter-tdTomato transgenic mice has been described elsewhere.[13] Twenty-five micrograms/body of BAp-A, BAp-E, or BAp-M dissolved in PBS was injected subcutaneously into TRAP-tdTomato mice once a day beginning 3 days prior to the recording of images. Intravital microscopy of mouse calvaria bone tissues was performed using a protocol modified from a previous study.[6] Mice were anesthetized with isoflurane (Escain; 2% vaporized in 100% oxygen), and the hair at the neck and scalp was removed with hair removal lotion (Kracie). The frontoparietal skull was exposed, and the mouse head was immobilized in a custom-designed stereotactic holder. The imaging system was composed of a multiphoton microscope (SP5; Leica) driven by a laser (Mai-Tai HP Ti: Sapphire; Spectraphysics) tuned to 900 nm and an upright microscope (DM6000B; Leica) equipped with a 20× water immersion objective (HCX APO, N.A. 1.0; Leica). The microscope was enclosed in an environmental chamber in which anesthetized mice were warmed by heated air. Fluorescent probes were detected through a bandpass emission filter at 525/50 nm. Osteoclasts were visualized by expression of TRAP-tdTomato (detected using a 585/40 nm filter). Snapshot images were acquired, and raw imaging data were processed with Imaris (Bitplane) with a Gaussian filter for noise reduction. In vivo imaging experiments were performed three times for each probe, and representative images are shown.

ASSOCIATED CONTENT

Supporting Information. Synthetic scheme, photophysical properties, and high-performance liquid chromatograms of BAps, and images of negative control experiment in vivo. This material is available free of charge via the Internet at http://pubs.acs.org.

AUTHOR INFORMATION

Corresponding Author
kkikuchi@mls.eng.osaka-u.ac.jp

ACKNOWLEDGMENT

This work was partially supported by the Japan Society for the Promotion of Science (JSPS) through its "Funding Program for World-Leading Innovative R&D on Science and Technology (FIRST) Program" and by the Ministry of Education, Culture, Sports, Science and Technology (MEXT) of Japan (Grant No. 22108519 and 20675004). K.K. and M.I. express their special thanks for support from the Takeda Science Foundation and the Mochida Memorial Foundation. K.K. also thanks the Naito Foundation for financial support. K.K. and S.M. acknowledge the Asahi Glass Foundation for financial support.

REFERENCES

(1) Boyle, W. J.; Simonet, W. S.; Lacey, D. L. *Nature* **2003**, *423*, 337–342.
(2) Raggatt, L. J.; Partridge, N. C. *J. Biol. Chem.* **2010**, *285*, 25103–25108.
(3) Teitelbaum, S. L. *Science* **2000**, *289*, 1504–1508.
(4) Rodan, G. A.; Martin, T. J. *Science* **2000**, *289*, 1508–1514.

(5) (a) Marks, K. M.; Nolan, G. P. *Nat. Methods* **2006**, *3*, 591–596. (b) Hinner, M. J.; Johnsson, K. *Curr. Opin. Biotechnol.* **2010**, *21*, 766–776. (c) Giepmans, B. N. G.; Adams, S. R.; Ellisman, M. H.; Tsien, R. Y. *Science* **2006**, *312*, 217–224. (d) Sadhu, K. K.; Mizukami, S.; Hori, Y.; Kikuchi, K. *ChemBioChem* **2011**, *12*, 1299–1308.

(6) Ishii, M.; Egen, J. G.; Klauschen, F.; Meier-Schellersheim, M.; Saeki, Y.; Vacher, J.; Proia, R. L.; Germain, R. N. *Nature* **2009**, *458*, 524–528.

(7) Kozloff, K. M.; Quinti, L.; Patntirapong, S.; Hauschka, P. V.; Tung, C.-H.; Weissleder, R.; Mahmoodet, U. *Bone* **2009**, *44*, 190–198.

(8) (a) Han, J.; Burgess, K. *Chem. Rev.* **2010**, *110*, 2709–2728. (b) Wang, R.; Yu, C.; Yu, F.; Chen, L. *Trends Anal. Chem.* **2010**, *29*, 1004–1013.

(9) (a) Roelofs, A. J.; Coxon, F. P.; Ebetino, F. H.; Lundy, M. W.; Henneman, Z. J.; Nancollas, G. H.; Sun, S.; Blazewska, K. M.; Bala, J. L. F.; Kashemirov, B. A.; Khalid, A. B.; McKenna, C. E.; Rogers, M. J. *J. Bone Miner. Res.* **2010**, *25*, 606–616. (b) Kashemirov, B. A.; Bala, J. L. F.; Chen, X.; Ebetino, F. H.; Xia, Z.; Russell, R. G. G.; Coxon, F. P.; Roelofs, A. J.; Rogers, M. J.; McKenna, C. E. *Bioconjugate Chem.* **2008**, *19*, 2308–2310. (c) Zaheer, A.; Lenkinski, R. E.; Mahmood, A.; Jones, A. G.; Cantley, L. C.; Frangioni, J. V. *Nat. Biotechnol.* **2001**, *19*, 1148–1154.

(10) (a) Loudet, A.; Burgess, K. *Chem. Rev.* **2007**, *107*, 4891–4932. (b) Ulrich, G.; Ziessel, R.; Harriman, A. *Angew. Chem., Int. Ed.* **2008**, *47*, 1184–1201.

(11) Urano, Y.; Asanuma, D.; Hama, Y.; Koyama, Y.; Barrett, T.; Kamiya, M.; Nagano, T.; Watanabe, T.; Hasegawa, A.; Choyke, P. L.; Kobayashi, H. *Nat. Med.* **2009**, *15*, 104–109.

(12) (a) Sunahara, H.; Urano, Y.; Kojima, K.; Nagano, T. *J. Am. Chem. Soc.* **2007**, *129*, 5597–5604. (b) Gabe, Y.; Urano, Y.; Kikuchi, K.; Kojima, H.; Nagano, T. *J. Am. Chem. Soc.* **2004**, *126*, 3357–3367.

(13) Kikuta, J.; Wada, Y.; Kowada, T.; Wang, Z.; Sun-Wada, G.-H.; Shimazu, Y.; Nishiyama, I.; Kubo, A.; Mizukami, S.; Maiya, N.; Yasuda, H.; Kikuchi, K.; Germain, R. N.; Ishii, M. Unpublished.

The sphingosine-1-phosphate transporter Spns2 expressed on endothelial cells regulates lymphocyte trafficking in mice

Shigetomo Fukuhara,[1] Szandor Simmons,[2,3] Shunsuke Kawamura,[2,3] Asuka Inoue,[4] Yasuko Orba,[5] Takeshi Tokudome,[6] Yuji Sunden,[7] Yuji Arai,[8] Kazumasa Moriwaki,[9] Junji Ishida,[10] Akiyoshi Uemura,[9] Hiroshi Kiyonari,[11] Takaya Abe,[11] Akiyoshi Fukamizu,[10] Masanori Hirashima,[9] Hirofumi Sawa,[5] Junken Aoki,[4] Masaru Ishii,[2,3] and Naoki Mochizuki[1]

[1]Department of Cell Biology, National Cerebral and Cardiovascular Center Research Institute, Osaka, Japan. [2]Laboratory of Cellular Dynamics, World Premier International Research Center–Immunology Frontier Research Center, Osaka University, Osaka, Japan. [3]Japan Science and Technology, Core Research for Evolutional Science and Technology (CREST), Tokyo, Japan. [4]Laboratory of Molecular and Cellular Biochemistry, Graduate School of Pharmaceutical Sciences, Tohoku University, Miyagi, Japan. [5]Department of Molecular Pathobiology, Hokkaido University Research Center for Zoonosis Control, Sapporo, Japan. [6]Department of Biochemistry, National Cerebral and Cardiovascular Center Research Institute, Osaka, Japan. [7]Laboratory of Comparative Pathology, Hokkaido University School of Veterinary Medicine, Sapporo, Japan. [8]Department of Molecular Biology, National Cerebral and Cardiovascular Center Research Institute, Osaka, Japan. [9]Division of Vascular Biology, Department of Physiology and Cell Biology, Kobe University Graduate School of Medicine, Hyogo, Japan. [10]Life Science Center, Tsukuba Advanced Research Alliance, University of Tsukuba, Ibaraki, Japan, and Graduate School of Life and Environmental Sciences, University of Tsukuba, Ibaraki, Japan. [11]Laboratory for Animal Resources and Genetic Engineering, RIKEN Center for Developmental Biology, Hyogo, Japan.

The bioactive lysophospholipid mediator sphingosine-1-phosphate (S1P) promotes the egress of newly formed T cells from the thymus and the release of immature B cells from the bone marrow. It has remained unclear, however, where and how S1P is released. Here, we show that in mice, the S1P transporter spinster homolog 2 (Spns2) is responsible for the egress of mature T cells and immature B cells from the thymus and bone marrow, respectively. Global *Spns2*-KO mice exhibited marked accumulation of mature T cells in thymi and decreased numbers of peripheral T cells in blood and secondary lymphoid organs. Mature recirculating B cells were reduced in frequency in the bone marrow as well as in blood and secondary lymphoid organs. Bone marrow reconstitution studies revealed that Spns2 was not involved in S1P release from blood cells and suggested a role for Spns2 in other cells. Consistent with these data, endothelia-specific deletion of *Spns2* resulted in defects of lymphocyte egress similar to those observed in the global *Spns2*-KO mice. These data suggest that Spns2 functions in ECs to establish the S1P gradient required for T and B cells to egress from their respective primary lymphoid organs. Furthermore, Spns2 could be a therapeutic target for a broad array of inflammatory and autoimmune diseases.

Introduction

Sphingosine-1-phosphate (S1P) is a bioactive lysophospholipid mediator that plays a crucial role in diverse physiological functions, such as lymphocyte trafficking, vascular development, and inflammation (1–5). S1P exerts biological functions mostly through activating cell-surface G protein–coupled receptors S1P1–S1P5, while intracellular S1P is also known to act as a second messenger to regulate inflammation (6). It remains unclear how intracellular S1P is transported to the outside of the cells to activate S1P receptors expressed on the cells.

The activation of S1P1 signaling in lymphocytes by S1P has been shown to promote the egress of newly formed T cells from the thymus and that of mature T and B cells from secondary lymphoid organs such as spleen and lymph nodes (7–10). An immunosuppressive molecule, FTY720, produces peripheral lymphopenia by blocking the lymphocyte egress from the thymus and lymph nodes. Interestingly, FTY720 was found to elicit the immunosuppressive effect by functionally antagonizing the S1P/S1P1 signaling pathway (8, 11–13). In fact, this compound has been recently approved by the United States Food and Drug Administration for treatment of autoimmune diseases (14). In addition, S1P/S1P1 receptor signals direct the release of immature B cells from the bone marrow to the peripheral blood (15, 16).

The concentration of S1P is abundant in circulatory fluids, such as blood and lymph (~μM), whereas it is normally kept low in the lymphoid tissues (~nM) by S1P-degrading enzymes that include lipid phosphate phosphatase 3 (17, 18). However, it has been suggested that this concentration difference of S1P is required but not sufficient for lymphocyte egress from lymphoid tissues into the circulation (9), implying the significance of S1P gradient made in lymphoid tissues. Consistently, S1P produced by neural crest–derived perivascular cells is required for efficient T cell egress (19). Moreover, lymphatic ECs release S1P, which is necessary for lymphocyte egress from lymph nodes into lymph (20). However, it is still unclear how B and T cell egress from the primary lymphoid organs and which cells release S1P that promotes the egress of these cells.

S1P is generated inside of the cell by phosphorylation of sphingosine in a reaction catalyzed by sphingosine kinase 1 and 2, 2 closely related isozymes, and is exported toward the outside of the cell to stimulate its cell-surface receptors (21, 22). Release of S1P is observed in a variety of cells, such as platelets, erythrocytes, mononuclear cells, neutrophils, mast cells, and ECs (3, 21–28). In vitro analyses have revealed that ABC transporters mediate S1P release in several types of cells, such as mast cells, erythrocytes, platelets, breast cancer cells, and

Conflict of interest: The authors have declared that no conflict of interest exists.
Citation for this article: *J Clin Invest.* 2012;122(4):1416–1426. doi:10.1172/JCI60746.

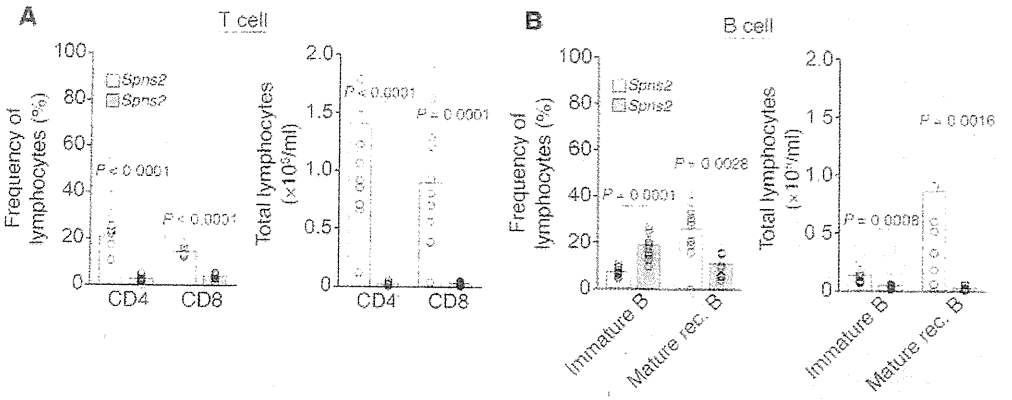

Figure 1

Mature T and recirculating mature B lymphocytes are remarkably reduced in the peripheral blood of *Spns2*$^{-/-}$ mice. (**A** and **B**) Flow cytometric analyses of control (*Spns2*$^{+/+}$) and global *Spns2*$^{-/-}$ mice. (**A**) Frequencies (left) and total numbers (right) of CD4 SP (CD4) and CD8 SP (CD8) T cells in peripheral blood are shown (n = 11). (**B**) Frequencies (left) and total numbers (right) of immature B cells (CD19$^+$CD23$^-$IgD$^-$IgM$^+$, immature B) and mature recirculating B cells (CD19$^+$CD23$^+$IgD$^+$, Mature rec. B) in peripheral blood are shown (n = 11). In **A** and **B**, bars and circles indicate averages and values for individual mice, respectively.

astrocytes (24, 29–32). We and others have identified the S1P transporter spinster homolog 2 (Spns2) as an S1P transporter in zebra fish (33, 34). However, the physiological functions of Spns2 in mammals remain totally unknown. Furthermore, S1P transporters responsible for S1P-mediated lymphocyte trafficking have not been identified.

In the present study, we investigated the importance of Spns2 in lymphocyte trafficking by analyzing the *Spns2*-deficient mice and found that Spns2 is responsible for egress of mature T cells and immature B cells from thymus and bone marrow, respectively. We further revealed, by performing bone marrow reconstitution studies and by analyzing mice with conditional deletion of Spns2 in ECs, that ECs release S1P through Spns2, thereby promoting lymphocyte egress from both thymus and bone marrow.

Results

Spns2 is essential for trafficking of both T and B cells. To address the physiological functions of Spns2 in mammals, we generated global *Spns2*-KO (*Spns2*$^{-/-}$) mice by crossing *Spns2*$^{f/f}$ mice, in which exon 2 of the *Spns2* gene is flanked with loxP sites, with mice expressing Cre recombinase under the control of cytomegalovirus promoter (Supplemental Figure 1; supplemental material available online with this article; doi:10.1172/JCI60746DS1). RT-PCR analyses of the RNA extracted from the lungs of WT and *Spns2*$^{-/-}$ mice revealed that *Spns2*$^{-/-}$ mice express a mutant mRNA transcript lacking exon 2–derived sequence encoding aa 124–145 of WT Spns2 (Supplemental Figure 2, A and B). This Spns2 mutant protein failed to localize at the plasma membrane and lost the ability to export S1P (Supplemental Figure 2, C and D). Thus, we conclude that *Spns2*$^{-/-}$ mice are indeed functionally disrupted for Spns2.

Spns2$^{-/-}$ mice develop normally, survive to adulthood, and are fertile, although they exhibited symblepharon to a greater or lesser extent (Supplemental Figure 3). In addition, blood biochemical examination revealed no significant differences between WT and *Spns2*$^{-/-}$ mice (Supplemental Figure 4). Notably, hematological analysis showed a significant decrease in white blood cell count in *Spns2*$^{-/-}$ mice compared with control mice, although there were no differences in the other hematological parameters, such as red blood cells, platelets, hemoglobin, hematocrit, mean corpuscular volume, mean corpuscular hemoglobin, and mean corpuscular hemoglobin concentration (Supplemental Figure 5), implying the role of Spns2 in lymphocyte trafficking.

It should be noted that the number and proportion of mature CD4 and CD8 single-positive (SP) T cells was dramatically reduced in the blood of *Spns2*$^{-/-}$ mice (Figure 1A and Supplemental Figure 6A). In addition, immature B cells (CD19$^+$CD23$^-$IgD$^-$IgM$^+$) and mature recirculating B cells (CD19$^+$CD23$^+$IgD$^+$) were decreased in the blood of *Spns2*$^{-/-}$ mice compared with WT mice (Figure 1B and Supplemental Figure 6B). These findings suggest that Spns2 is involved in trafficking of both T and B lymphocytes.

Spns2 regulates T cell egress from the thymus into blood. To study the cause of the decrease in mature T lymphocytes in the blood of *Spns2*$^{-/-}$ mice, we examined the thymus where T lymphocytes develop and from which they egress into blood. *Spns2*$^{-/-}$ mice exhibited normal thymus structures (Supplemental Figure 7). The numbers and proportions of mature CD4 and CD8 SP T cells in the thymi of *Spns2*$^{-/-}$ mice were increased compared with those of WT mice, although there was no significant change in the number of immature CD4/CD8 double-positive (DP) T cells and CD4/CD8 double-negative (DN) progenitor thymocytes (Figure 2, A and B). These data suggest a significant role for Spns2 in modulating the egress of mature T cells from the thymus into the blood.

During final maturation of CD4 and CD8 SP T cells in the medulla of the thymus, they downregulate CD69, upregulate S1P1 and CD62L, and consequently migrate out of the thymus in response to S1P (35–38). Thus, we examined the semi-mature (CD69$^+$CD62L$^{lo/-}$) and fully mature (CD69$^{lo/-}$CD62L$^+$) SP T cells in the thymi of *Spns2*$^{-/-}$ mice. The proportion of fully mature SP T cells was increased in comparison with that of WT mice, while the relative amount of semi-mature SP T cells was decreased (Supplemental Figure 8, A and B). In addition, the cell-surface expression of CD69 on the fully mature SP T cells was slightly higher in *Spns2*$^{-/-}$ mice than in WT mice (Supplemental Figure 8C). Since S1P is suggested to be required for full CD69 downregulation during final maturation of SP thymocytes (8, 36, 39), this may be due to a decreased release of S1P in thymus of *Spns2*$^{-/-}$ mice. These results indicate that Spns2 is involved in the release of S1P required for T cell egress from the thymus into the blood.

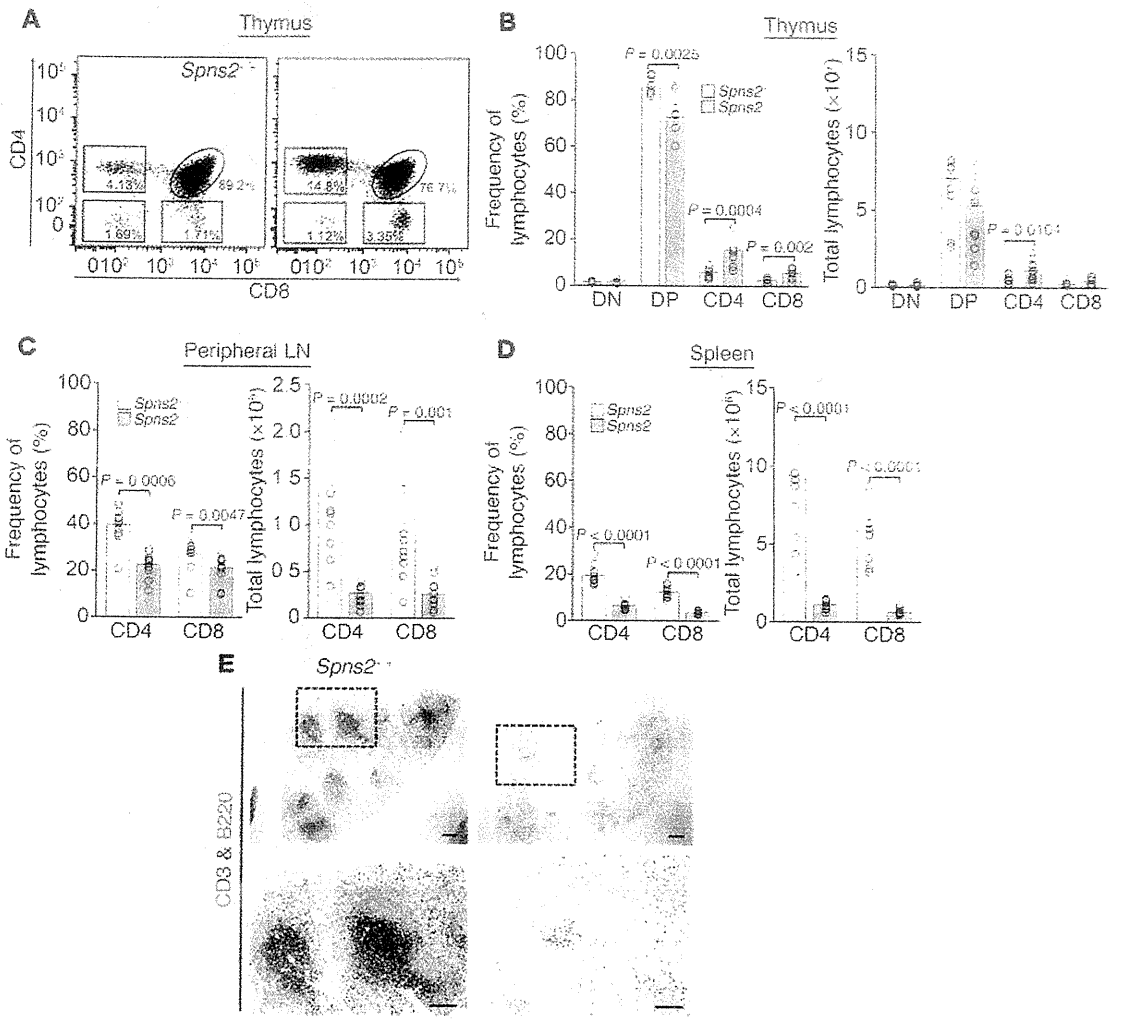

Figure 2

Egress of mature T cells from the thymus is impaired in *Spns2*$^{-/-}$ mice. (**A–D**) Flow cytometric analyses of control (*Spns2*$^{+/+}$) and global *Spns2*$^{-/-}$ mice. (**A**) A representative flow cytometric analysis of T cells in the thymus. The numbers represent the percentages of CD4 SP, CD8 SP, CD4/CD8 DP T cells, and CD4/CD8 DN thymocytes. (**B**) Frequencies (left) and total numbers (right) of CD4/CD8 DN (DN), CD4/CD8 DP (DP), CD4 SP (CD4) and CD8 SP (CD8) thymocytes and T cells are shown (n = 11). (**C**) Frequencies and numbers of CD4 SP (CD4) and CD8 SP (CD8) T cells in peripheral lymph nodes are shown (n = 11). (**D**) Frequencies and numbers of CD4 SP (CD4) and CD8 SP (CD8) T cells in spleens are shown (n = 11). In **B–D**, bars and circles indicate averages and values for individual mice, respectively. (**E**) Spleen sections from control (*Spns2*$^{+/+}$) or *Spns2*$^{-/-}$ mice, stained to detect CD3$^+$ T cells (blue) and B220$^+$ B cells (red). The boxed areas of upper panels are enlarged in lower panels. Scale bars: 200 μm (top row); 50 μm (bottom row).

To assess the possibility that lack of mature T cells in the blood of *Spns2*$^{-/-}$ mice is related to their accumulation in other secondary lymphoid tissues, we further examined mature SP T lymphocytes in peripheral lymph nodes and in the spleen. In contrast with the accumulation of mature T cells in the thymus, the numbers and proportions of mature CD4 and CD8 SP T cells were dramatically reduced in peripheral lymph nodes and in the spleen of *Spns2*$^{-/-}$ mice, although their structures were normal (Figure 2, C–E, and Supplemental Figure 7). These results show that a decrease in the number of mature T cells in the peripheral blood of *Spns2*$^{-/-}$ mice is a consequence of impaired T cell egress from the thymus, but not due to the accumulation in the secondary lymphoid organs.

Spns2 regulates egress of immature B cells from the bone marrow into the blood. In the late stage of B cell development in the bone marrow, newly generated immature B cells are exported into the peripheral blood in an S1P/S1P1 signal-dependent manner (15, 16). The immature B cells subsequently undergo maturation in the secondary lymphoid tissues and migrate back to the bone marrow through the blood (recirculating mature B cells). To explore the cause of remarkable reduction of recirculating mature B lymphocytes in the peripheral blood of *Spns2*$^{-/-}$ mice, we examined the number and proportion of the lymphocytes at different developmental stages. The numbers and frequencies of mature recirculating B cells (B220^{hi}IgM$^+$ or CD19$^+$IgM$^+$IgD$^+$) were significantly reduced in the bone marrow of *Spns2*$^{-/-}$ mice compared with that of control mice (Figure 3, A and B, and Supplemental Figure 9). However, the number of pro-/pre-B cells (B220$^+$IgM$^-$) and immature B cells (B220^{lo}IgM$^+$ or CD19$^+$IgM$^+$IgD$^-$) was normal in the bone marrow of *Spns2*$^{-/-}$ mice, although their frequencies were slightly

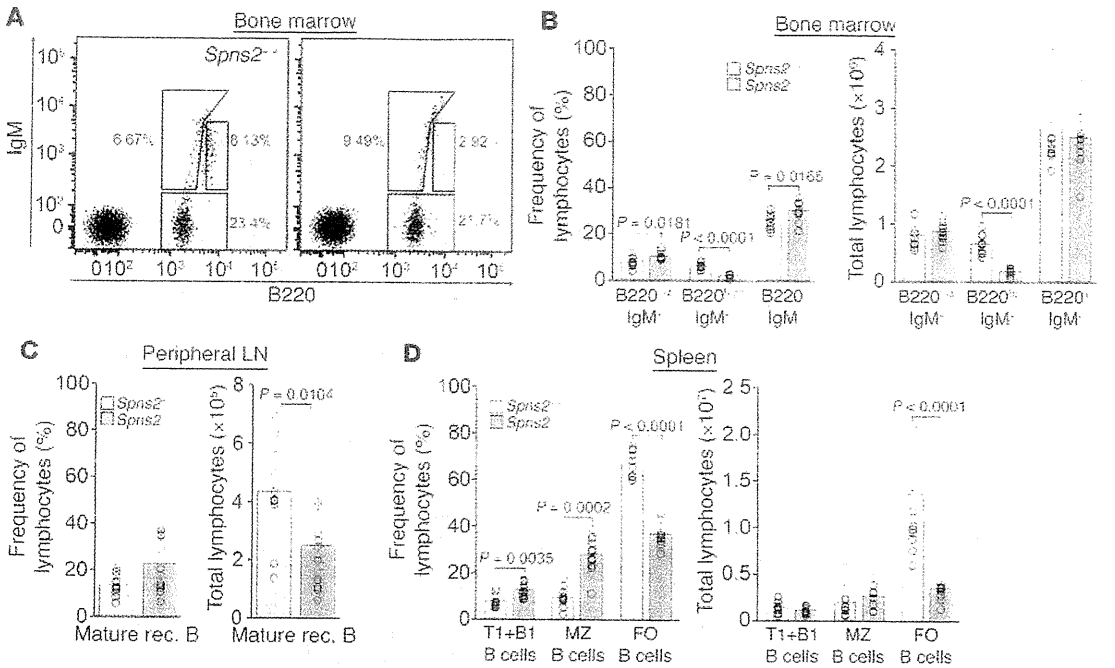

Figure 3

Immature B cell egress from bone marrow is impaired in *Spns2*$^{-/-}$ mice. (**A–D**) Flow cytometric analysis of B cells in control (*Spns2*$^{+/+}$) and *Spns2*$^{-/-}$ mice. (**A**) A representative flow cytometric analysis of progenitor B (B220^{+}IgM^{-}), immature B (B220^{lo}IgM^{+}) and mature recirculating B cells (B220^{hi}IgM^{+}) in the bone marrow cavity. Numbers indicate the percentages of IgM- and B220-expressing cells of total lymphocytes. (**B**) Frequencies (left) and total numbers of pro–/pre–B cells (B220^{+}IgM^{-}), immature B cells (B220^{lo}IgM^{+}), and mature recirculating B cells (B220^{hi}IgM^{+}) defined as in **A** are shown (n = 11). (**C**) Frequencies (left) and numbers (right) of mature recirculating B (mature rec. B) cells (CD19^{+}CD23^{+}IgD^{+}) in peripheral lymph nodes are shown (n = 11). (**D**) Frequencies (left) and numbers (right) of T1 B cells (CD19^{+}CD21^{-}CD23^{-}), MZ (CD19^{+}CD21^{+}CD23^{lo}), and follicular B cells (FO) CD19^{+}CD21^{lo}CD23^{+}) in spleens are shown (n = 11). In **B–D**, bars and circles indicate averages and values for individual mice, respectively.

higher than those in control mice, probably due to the reduction of mature recirculating B cell count (Figure 3, A and B, and Supplemental Figure 9). Together with the evidence for the decreased number of immature B cells in the peripheral blood of *Spns2*$^{-/-}$ mice (Figure 1B), these results suggest that the egress of immature B cells from the bone marrow is impaired in *Spns2*$^{-/-}$ mice.

To further confirm this conclusion, we examined the number and proportion of B lymphocytes in the secondary lymphoid organs. In the peripheral lymph nodes, the number of mature B cells was reduced in *Spns2*$^{-/-}$ mice, although the frequency of mature B cells was not different from that in control mice (Figure 3C). In the spleen, the numbers and proportions of follicular B cells were significantly decreased in *Spns2*$^{-/-}$ mice compared with those of control mice, although there was no difference in the number of marginal zone (MZ) and transitional type 1 (T1) and B1 B cells between control and *Spns2*$^{-/-}$ mice (Figure 3D). These results reveal that the decrease in mature recirculating B cells in the peripheral blood of *Spns2*$^{-/-}$ mice is not due to their accumulation in the secondary lymphoid organs, although it remains unclear whether Spns2 is involved in the egress of B lymphocytes from the secondary lymphoid organs. Therefore, we conclude that Spns2 is required for the egress of immature B cells from the bone marrow into the blood.

Spns2 is not involved in S1P release from blood cells. Which cells expressing Spns2 are responsible for releasing S1P necessary for lymphocyte trafficking? Blood cells, especially erythrocytes, are known to produce S1P, thereby contributing to high plasma S1P concentration (9, 23–26). Thus, we first investigated whether Spns2 is involved in S1P release from blood cells. In *Spns2*$^{-/-}$ mice, plasma S1P levels were reduced to 54% of those in control mice (0.39 ± 0.03 μM in control mice; 0.21 ± 0.01 μM in *Spns2*$^{-/-}$ mice), although plasma sphingosine and glycerolysophospholipids of *Spns2*$^{-/-}$ mice were comparable to those in control mice (Figure 4, A–H). Most of the plasma S1P is known to be associated with HDL and albumin (40–42). Consistent with the reduced concentration of plasma S1P in *Spns2*$^{-/-}$ mice, the amount of S1P associated with HDL and albumin was lower in *Spns2*$^{-/-}$ mice than in WT mice (Supplemental Figure 10).

To further clarify whether the reduction of plasma S1P concentration in *Spns2*$^{-/-}$ mice is attributed to the decreased S1P release from blood cells, we examined the secretion of S1P from blood cells isolated from either control or *Spns2*$^{-/-}$ mice. S1P release from blood cells occurred in *Spns2*$^{-/-}$ mice to an extent similar to that in control mice (Figure 5A). This S1P release was not caused by membrane damage, since no release was observed when the cells were incubated at 4°C (Figure 5A), as previously reported (27). These results suggest that Spns2 is not involved in the release of S1P from blood cells. To further confirm this conclusion, we performed bone marrow reconstitution studies (Supplemental Figure 11). Reconstitution of irradiated *Spns2*$^{-/-}$ mice with WT bone marrow did not restore the reduced concentration of plasma S1P (Figure 5B). Furthermore, *Spns2*$^{-/-}$ mice reconstituted with WT bone marrow still exhibited accumulation of mature SP T lymphocytes in the thymus and reduction of mature recirculating B cells in the bone marrow in comparison with WT mice (Figure 5,

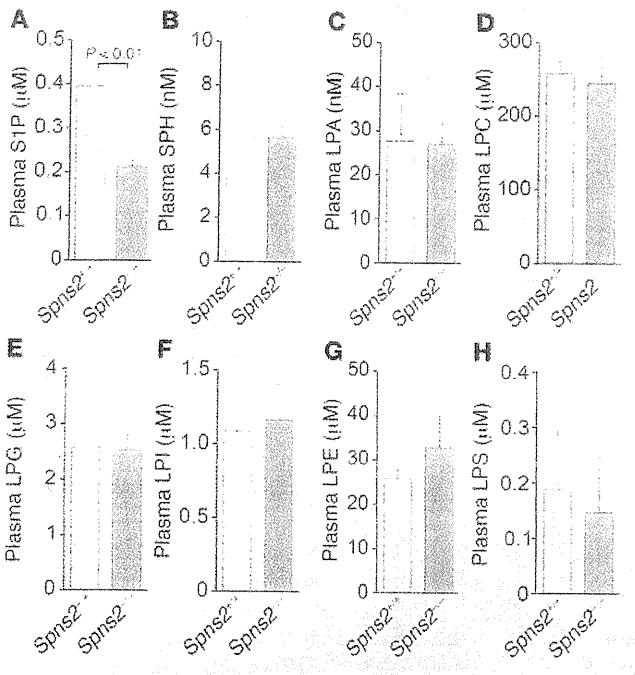

Figure 4
Plasma S1P concentration is reduced in *Spns2*$^{-/-}$ mice. (**A–H**) Plasma concentrations of S1P (**A**), sphingosine (SPH) (**B**), LPA (**C**), LPC (**D**), LPG (**E**), LPI (**F**), LPE (**G**), and LPS (**H**) in control (*Spns2*$^{+/+}$) or *Spns2*$^{-/-}$ mice. Data are shown as mean ± SD (n = 3–5).

C and D). These findings indicate that cells other than blood cells expressing Spns2 secrete S1P to control lymphocyte trafficking.

Spns2 mediates S1P release from ECs. Cultured vascular ECs produce S1P in vitro (43, 44), although S1P release from vascular ECs has not been confirmed in vivo. Another type of EC, lymphatic ECs, secrete S1P into lymph, thereby regulating lymphocyte egress from lymph nodes (20). Thus, we next investigated whether Spns2 is involved in the release of S1P from ECs. RT-PCR analyses revealed that Spns2 is expressed not only in lymphatic ECs, but also in several types of vascular ECs (Figure 6A). In addition, depletion of Spns2 by siRNA resulted in the inhibition of S1P release from ECs (Figure 6, B and C). Furthermore, we investigated whether Spns2 is expressed in ECs in vivo by performing in situ hybridization analyses. *Spns2* mRNA was clearly expressed on the ECs in the thymus (Figure 6D). Although it has been reported that pericytes covering thymic ECs release S1P to promote T cell egress from thymus (19), we could not detect expression of *Spns2* mRNA on the pericytes in the thymus (Figure 6D). Besides the thymus, expression of *Spns2* mRNA was also observed in the ECs of other tissues, such as heart, lung, and hypothalamus, but not in those of kidney and olfactory bulb (Supplemental Figure 12). These results suggest that ECs secrete S1P through Spns2. Hence, we hypothesized that S1P released from ECs via Spns2 is required for lymphocyte egress from primary lymphoid organs.

ECs regulate thymic egress by releasing S1P through Spns2. To address whether Spns2 functions in ECs to regulate lymphocyte trafficking, we tried to generate mice lacking Spns2 in ECs (Spns2-ECKO: *Spns2*$^{f/f}$*;Tie2Cre*) by crossing the *Spns2*$^{f/f}$ mice with the mice expressing Cre recombinase under the Tie2 promoter (Supplemental Figure 1). In Spns2-ECKO mice, plasma S1P concentration was decreased to the level observed in *Spns2*$^{-/-}$ mice (Supplemental Figure 13), indicating that ECs release S1P into plasma in an Spns2-dependent manner. Spns2-ECKO mice develop normally without symblepharon formation that is observed in global *Spns2*$^{-/-}$ mice, suggesting that Spns2 acts as an S1P transporter not only in ECs but also in other types of cells.

We further investigated whether Spns2 functions in ECs to promote T cell egress from the thymus by S1P. Compared with control mice, the proportion of mature CD4 and CD8 SP T cells was increased in the thymus of Spns2-ECKO mice, but to a lesser extent than that in *Spns2*$^{-/-}$ mice (Figure 2A and Figure 7A). In addition, the number and proportion of CD4 and CD8 SP T cells in Spns2-ECKO mice were dramatically decreased in the peripheral blood, spleen, and peripheral lymph nodes (Figure 7, B and C, and Supplemental Figure 14), suggesting an impaired thymic egress of mature T lymphocytes in Spns2-ECKO mice into the peripheral lymphoid organs. The Tie2 promoter is active not only in ECs, but also in hematopoietic cells (45–47). To further confirm that the phenotype of Spns2-ECKO mice is attributed to the impaired function of Spns2 in ECs, we performed bone marrow reconstitution experiments. Spns2-ECKO mice reconstituted with control bone marrow exhibited accumulation of mature CD4 and CD8 SP T cells in the thymus, and their deficiency in the peripheral blood compared with control mice reconstituted with control bone marrow (Supplemental Figure 15). These findings apparently reveal that S1P released from ECs through Spns2 is involved in the egress of mature T cells from the thymus into the blood.

ECs promote the egress of immature B cells from the bone marrow by releasing S1P through Spns2. We further investigated the role of ECs in immature B cell egress from the bone marrow. As observed in *Spns2*$^{-/-}$ mice, the numbers and proportions of mature recirculating B cells, but not pro–/pre–B cells and immature B cells, were remarkably decreased in the bone marrow of Spns2-ECKO mice in comparison with control mice (Figure 8A and Supplemental Figure 16). Mature recirculating B cells in the blood and peripheral lymph nodes of Spns2-ECKO mice were decreased (Figure 8B and Supplemental Figure 17). Furthermore, the numbers and frequencies of follicular B cells were significantly reduced in the spleen of Spns2-ECKO mice compared with control mice (Figure 8C), although the number of MZ B cells in the spleen was comparable between WT and Spns2-ECKO mice. Unexpectedly, the spleens of Spns2-ECKO mice have increased numbers of T1 and B1 B cells compared with those of control mice. This result may imply a more complex role of Spns2 in B cell trafficking that has to be tested in more detail in further experiments. Moreover, reconstitution of irradiated Spns2-ECKO mice with control bone marrow did not restore reduction of mature recirculating B cells in the bone marrow and peripheral blood (Supplemental Figure 18). These results demonstrate that S1P released by ECs through Spns2 promotes the egress of immature B cells from the bone marrow into the blood.

Discussion

In the present study, we show for what we believe is the first time that Spns2 expressed on ECs is essential for lymphocyte egress from the primary lymphoid organs. By analyzing the *Spns2*-deficient mice, we found that Spns2 is an S1P transporter required for the egress of mature T cells and immature B cells from the thymus and the bone marrow, respectively, into the peripheral blood. In addition, by deleting Spns2 in ECs and performing bone marrow reconstitution studies, we showed that Spns2 regulates S1P secretion in ECs, but not in blood cells, to promote lymphocyte egress from primary lymphoid organs. Therefore, the

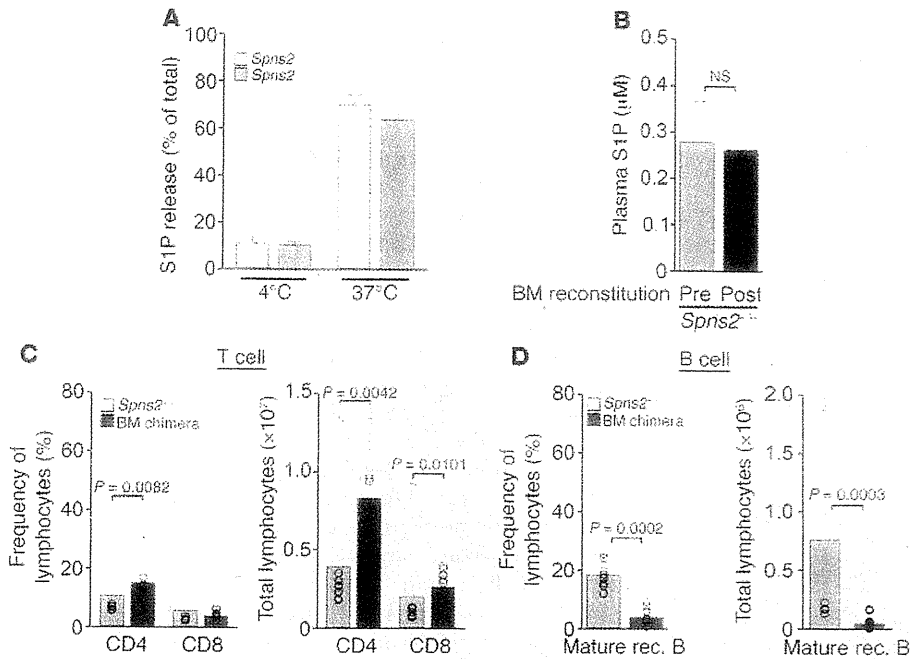

Figure 5

Spns2 is not involved in S1P release from blood cells. (**A**) Release of S1P by the blood cells isolated from control (*Spns2*$^{+/+}$) and *Spns2*$^{-/-}$ mice. Cells were incubated at either 4°C or at 37°C for 90 minutes as indicated at the bottom. Data are expressed as a percentage of the total amount of S1P in the cells without incubation and shown as mean ± SD (n = 4). (**B–D**) *Spns2*$^{-/-}$ mice were lethally irradiated and reconstituted with bone marrow from littermate control mice. (**B**) Plasma S1P concentrations of either *Spns2*$^{-/-}$ mice (Pre) or of those reconstituted with WT bone marrow (Post) (n = 13). (**C** and **D**) Flow cytometric analyses of control (*Spns2*$^{+/+}$) and *Spns2*$^{-/-}$ mice reconstituted with littermate control bone marrow (BM chimera). (**C**) Frequencies (left) and total numbers (right) of CD4 SP (CD4) and CD8 SP (CD8) T cells in the thymus are shown (*Spns2*$^{+/+}$, n = 8; BM chimera, n = 13). (**D**) Frequencies (left) and total numbers of mature recirculating B cells (CD19$^+$IgM$^+$IgD$^+$) in the bone marrow are shown (*Spns2*$^{+/+}$, n = 8; BM chimera, n = 13).

present study on Spns2 largely contributes to the understanding of S1P signaling, which is used in the egress of lymphocytes from primary lymphoid organs (1, 2, 4, 5).

Spns2 is the first S1P transporter functioning in mammals. Intracellularly generated S1P has to be transported out of the cell to stimulate its cell-surface receptors. Several lines of evidence obtained from in vitro studies have suggested the involvement of the ABC family of transporters in S1P release from several types of cells (22, 24, 29–32). However, their biological significance in vivo has remained unclear. In this study, we demonstrate Spns2 as a key S1P transporter that regulates lymphocyte trafficking in mammals. Although Spns2 regulates lymphocyte trafficking by inducing the release of S1P from ECs, this transporter may also function in other cells, since symblepharon was observed in *Spns2*$^{-/-}$ mice, but not in Spns2-ECKO mice. On the other hand, Spns2 appears not to be the only transporter of S1P in mammals because plasma S1P levels were partially but not completely decreased in *Spns2*$^{-/-}$ mice compared with control mice. Although blood cells, especially erythrocytes, are thought to be the major cellular source of S1P in plasma (9, 23, 27), blood cells from *Spns2*$^{-/-}$ mice still retained the ability to release S1P (Figure 5A). Thus, S1P release from blood cells appears to be mediated by S1P transporters other than Spns2. In addition, S1P transporters other than Spns2 might also be involved in the release of S1P required for vascular development, since *Spns2*$^{-/-}$ mice did not show the defects in vascular development that can be observed in *S1p1*-deficient mice (48).

This study clearly reveals that Spns2-dependent S1P release from ECs is important for egress of mature T cells from the thymus into the peripheral blood. Thymic egress is strictly controlled by the S1P/S1P1 signaling pathway (1, 2, 4, 5). In the thymus, thymocytes differentiate into mature T cells, and subsequently express S1P1 through upregulation of Krüppel-like factor 2 (5, 49). S1P1-expressing mature T cells acquire responsiveness to S1P, thereby exiting from the thymus into the peripheral blood. Until recently, it has been assumed that the S1P gradient between the thymus and the blood is required for egress of mature T cells. However, recent evidence has suggested that plasma S1P is insufficient to promote thymic egress (9, 19). Importantly, egress of mature T cells from the thymus was impaired in *Spns2*$^{-/-}$ mice even though the plasma contains enough concentration of S1P to stimulate lymphocyte S1P1 in vitro (10). Similarly, Zachariah and Cyster have recently reported that neural crest–derived pericytes covering the ECs release S1P responsible for thymic egress without influencing plasma S1P concentration (19). Therefore, mature T cells might be recruited to the abluminal side of blood vessels by S1P locally released from both ECs and pericytes, and possibly exit into the peripheral blood in response to high concentrations of plasma S1P. However, further studies are needed to confirm this hypothesis.

Spns2 expressed on ECs of the blood vessels is also essential for B cell egress from the bone marrow. Although recent reports reveal the role of S1P/S1P1 signaling in the egress of immature B cells from the bone marrow (15, 16), a cellular source of S1P involved in this process has not been identified. In *Spns2*$^{-/-}$ mice, the number of mature recirculating B cells was significantly decreased not only in the bone marrow but also in the blood, spleen, and peripheral lymph nodes, indicating a block in the egress of immature B cells from the bone marrow. Importantly, reconstitution of irradiated *Spns2*$^{-/-}$ mice with WT bone marrow did not rescue the deficiency of mature recirculating B cells in the bone marrow. Furthermore, Spns2-ECKO mice also exhibited reduced numbers of mature recirculating B cells in the bone marrow, peripheral blood, spleen, and peripheral lymph nodes, as observed in *Spns2*$^{-/-}$ mice. This phenotype was not rescued by reconstitution with control bone marrow. Thus, these results reveal for what we believe is the first time that ECs are the major cellular source of S1P necessary for the egress of immature B cells from the bone marrow. In the late stage of B cell development in the bone marrow, newly generated immature B cells placed in the parenchyma are first recruited into the sinusoidal compartment and subsequently

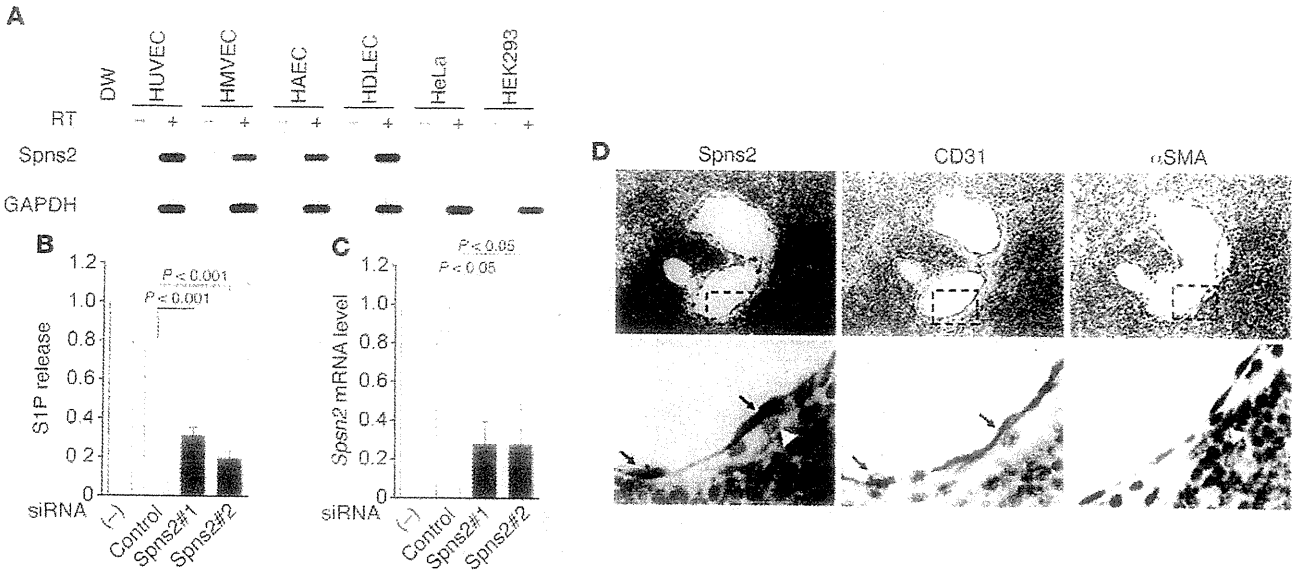

Figure 6

Spns2 is involved in S1P release from ECs. (**A**) Expression of Spns2 in ECs. RT-PCR analysis was performed to examine the expression of Spns2 in HUVECs, HMVECs, HAECs, HDLECs, HeLa, and HEK293 cells as indicated at the top. PCR was performed using specific primers for either Spns2 (upper panel) or GAPDH (lower panel). To verify the absence of contaminating genomic DNA, RT-PCR was also performed in the absence of reverse transcriptase (–). (**B** and **C**) S1P release from Spns2-depleted ECs. (**B**) Release of S1P by ECs transfected without (–) or with either control siRNA (control) or 2 independent siRNAs targeting Spns2 (Spns2#1 and Spns2#2). (**C**) Real-time RT-PCR analysis to assess the efficiency of siRNA-mediated Spns2 knockdown. In **B** and **C**, data are expressed relative to those observed in the untransfected cells and shown as mean ± SD of 3 independent experiments. (**D**) In situ hybridization for *Spns2* mRNA in thymus. Antisense probe was hybridized to thymus section (Spns2: purple). Serial sections were also stained with anti-CD31 (CD31: brown) and anti–α-SMA (brown) antibodies to identify ECs and pericytes, respectively. The boxed areas of upper panels are enlarged in lower panels. Arrows and white arrowheads indicate ECs and pericytes, respectively. Scale bars: 50 μm (upper panels); 10 μm (lower panels).

exported into the peripheral blood (50–52). Sinusoidal entry of immature B cells is thought to be a key step in bone marrow egress. Recently, it has been reported that S1P/S1P1 signaling promotes the movement of immature B cells from parenchyma to sinusoid, thereby facilitating egress of immature B cells from bone marrow (15, 16). Thus, bone marrow sinusoidal ECs may attract immature B cells from the parenchyma by producing S1P through Spns2 and thereby promoting the immature B cell egress into the peripheral blood.

The lymphocyte egress from secondary lymphoid organs such as lymph nodes and spleen also depends on S1P/S1P1 signaling. Pham et al. have recently reported that lymphatic ECs are an in vivo source of S1P required for lymphocyte egress from lymph nodes and Peyer patches (20). Since Spns2 is expressed not only in vascular ECs but also in lymphatic ECs, Spns2 may also regulate lymphocyte egress from lymph nodes by inducing the release of S1P from lymphatic ECs. However, to address this hypothesis, we need to analyze mice lacking Spns2 specifically in the lymphatic ECs because lymphocyte egress from primary lymphoid organs is severely impaired in global *Spns2*$^{-/-}$ mice. It also remains elusive whether Spns2 is involved in lymphocyte egress from spleen. Thus, this will be a subject for future studies.

In conclusion, we demonstrate that Spns2 is a key S1P transporter involved in lymphocyte trafficking and further indicate that vascular ECs are the major source of S1P in vivo responsible for lymphocyte egress from the thymus and the bone marrow. Thus, this study not only reveals the crucial role of Spns2 as an S1P transporter in mammals, but also contributes to our understanding of molecular mechanisms of S1P-mediated lymphocyte trafficking. Since S1P signaling is profoundly involved in the inflammatory and autoimmune diseases, such as multiple sclerosis, psoriasis, asthma, and rheumatoid arthritis, as well as in transplantation, Spns2 can be a potential therapeutic target for these diseases.

Methods

Generation of Spns2$^{f/f}$ *mice.* *Spns2*$^{f/f}$ mice (acc. no. CDB0705K; http://www.cdb.riken.jp/arg/mutant%20mice%20list.html), in which exon 2 is flanked by 2 loxP sites, were generated (Supplemental Figure 1A). TT2 ES cells derived from an F1 hybrid of C57BL/6 and CBA mice (53) were transfected with the targeting vector, selected in the presence of G418, and screened for homologous recombination by PCR and Southern blotting. Two ES clones were introduced into host embryos to generate chimeric mice. Chimeric mice with a high ES cell contribution were bred with the CMV-Cre mice (C57BL/6 strain background) expressing Cre recombinase under the control of cytomegalovirus promoter to generate heterozygous *Spns2*$^{+/-}$ mice (Supplemental Figure 1). *Spns2*$^{+/-}$ mice were intercrossed to obtain *Spns2*$^{-/-}$ mice (75% C57BL/6 and 25% CBA genetic background). The chimeric mice were also crossed with the CMV-Flp mice (C57BL/6 strain background) expressing Flp recombinase under the control of cytomegalovirus early enhancer/chicken β-actin promoter to remove the PKG-Neo-pA cassette, resulting in Spns2 floxed mice (Supplemental Figure 1). To inactivate the *Spns2* gene in ECs, the Spns2 floxed mice were bred with Tie2-Cre mice (C57BL/6 strain background), which carry the Cre recombinase driven by the Tie2 promoter (45, 46) and were provided by T.N. Sato (Nara Institute of Science and Technology, Nara, Japan) and M. Yanagisawa (University of Texas Southwestern Medical Center, Dallas, Texas, USA) (Supplemental Figure 1). For confirmation of cor-

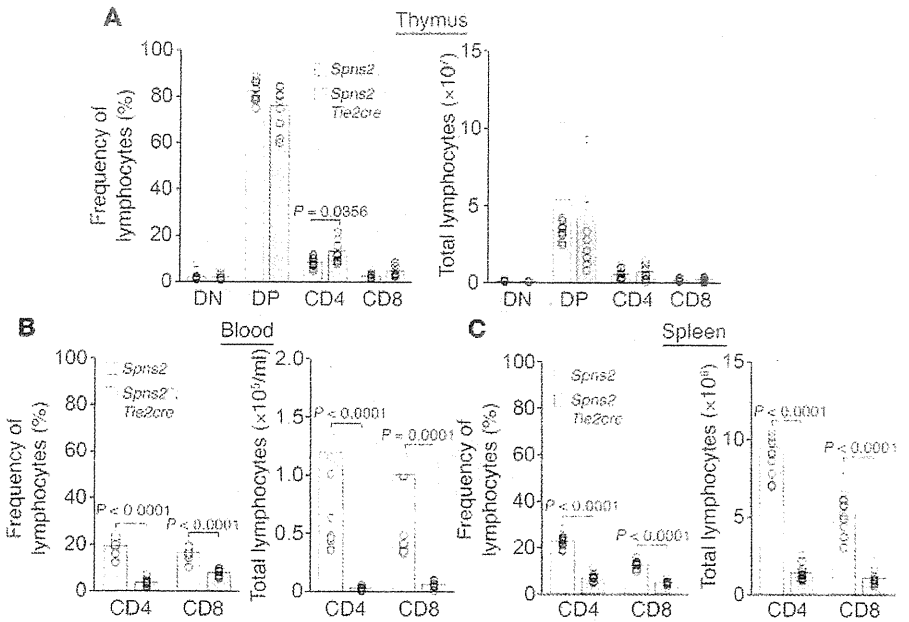

Figure 7
Spns2 expressed in ECs is required for mature T cell egress from thymus. (**A–C**) Flow cytometric analyses of lymphocytes of control (*Spns2$^{f/f}$*) or Spns2-ECKO (*Spns2$^{f/f}$;Tie2Cre*) mice. (**A**) Frequencies (left) and numbers (right) of CD4/CD8 DN (DN), CD4/CD8 DP (DP), CD4 SP (CD4), and CD8 SP (CD8) thymocytes and T cells in thymus are shown ($n = 11$). (**B**) Frequencies and numbers of CD4 SP (CD4) and CD8 SP (CD8) T cells in peripheral lymph nodes are shown ($n = 11$). (**C**) Frequencies and numbers of CD4 SP (CD4) and CD8 SP (CD8) T cells in spleens are shown ($n = 11$). In **A–C**, bars and circles indicate averages and values for individual mice, respectively.

rect targeting, Southern blot analysis was performed with the probe located outside of the regions used in the targeting vector (Supplemental Figure 1). For the genotyping of mice, PCR was performed using a forward primer, 5′-AGGCTCATTTCATGGCTGAT-3′, and a reverse primer, 5′-AGCCCTGTGCTCTCTGTTGT-3′, producing products of 552-bp fragment for WT allele, 842-bp fragment for floxed allele, and 316-bp fragment for deleted allele. All mice were housed under specific pathogen–free conditions.

RT-PCR and real-time RT-PCR. To check the expression of *Spns2* mRNA in *Spns2*$^{-/-}$ mice, total RNA was extracted from the lungs using TRIzol reagent (Invitrogen) and reverse transcribed by random hexamer primers using Superscript II (Invitrogen) according to the manufacturer's instructions. PCR amplification was carried out with the following primer sets: PCR1, 5′-AAGAGGTGCAGACGTTGTCC-3′ and 5′-CCACAGCTGAGGATCACCTT-3′, for exons 1–3 of the mouse *Spns2*; and PCR2, 5′-ATGATGTGCCTGGAATGC-3′ and 5′-TCAGACTTTCACGGATGCAG-3′, for complete coding sequence of mouse *Spns2*.

To determine the expression of Spns2 in ECs, RT-PCR was performed using the gene-specific primers for human *SPNS2* (5′-ACTTTGGGGTCAAGGACCGA-3′ and 5′-AATCACCTTCCTGTTGAAGCG-3′). Amplification of GAPDH was also performed using the gene-specific primers for human *GAPDH* (5′-ATGGGGAAGGTGAAGGTCG-3′ and 5′-GGGGTCATTGATGGCAACAATA-3′) in parallel as a control.

To assess the efficiency of siRNA-mediated knockdown of Spns2, total RNA was extracted from HUVECs transfected without or with either control siRNA or 2 independent siRNAs targeting Spns2 and subjected to quantitative real-time RT-PCR analysis using the QuantiFast SYBR Green RT-PCR Kit (QIAGEN) as described (54). For each reaction, 100 ng of total RNA was transcribed for 10 minutes at 50°C, followed by a denaturation step at 95°C for 5 minutes, 40 cycles of 10 seconds at 95°C, and 30 seconds at 60°C. Fluorescence data were collected and analyzed using Mastercycler ep realplex (Eppendorf). For normalization, expression of human *GAPDH* was determined in parallel as an endogenous control. The gene-specific primers used to amplify human *SPNS2* and *GAPDH* were the same as described above.

Cell culture, transfection, and siRNA-mediated gene silencing. HUVECs, human microvascular ECs (HMVECs), and human aortic ECs (HAECs) were purchased from Kurabo and maintained as described previously (55). Human dermal lymphatic ECs (HDLECs) were obtained from Lonza and maintained in EC growth medium EGM-2 (Lonza). HeLa and HEK293 cells were cultured in DMEM (Nissui) supplemented with 10% fetal bovine serum and antibiotics (100 μg of streptomycin/ml and 100 U of penicillin/ml).

Stealth siRNAs targeted to human Spns2 (HSS151335 and HSS151336) were purchased from Invitrogen. As a control, siRNA duplexes with irrelevant sequences were used. HUVECs were transfected with 20 nM siRNA duplexes using Lipofectamine RNAi MAX reagent (Invitrogen). After incubation for 48 hours, the cells were used for the experiments.

Detection of subcellular localization of GFP-tagged Spns2. cDNAs encoding WT and mutant Spns2 were amplified using cDNAs derived from the lungs of WT and *Spns2*$^{-/-}$ mice by RT-PCR, and cloned into pEGFP-N1 vector to construct the expression plasmids encoding WT and mutant Spns2 with a C-terminal GFP tag, respectively. HUVECs were transfected with the plasmid encoding either WT or mutant Spns2-GFP or with myristoylated GFP-encoding plasmid. GFP and phase contrast images were obtained using an IX81 inverted microscope (Olympus) equipped with a pE-1 LED excitation system (CoolLED).

S1P release from cultured cells. HEK293 cells were plated in 24-well plates (5×10^4 cells/well), cultured for 24 hours, and transfected with the expression plasmids indicated in the legend of Supplemental Figure 2D using Lipofectamine 2000 reagent (Invitrogen). After incubation for 24 hours, cells were incubated in 250 μl of serum-free DMEM containing 0.5 % fatty acid–free bovine serum albumin, 10 mM sodium glycerophosphate, 5 mM sodium fluoride, and 1 mM semicarbazide for 24 hours. To determine the role of Spns2 in S1P release from ECs, HUVECs transfected without or with either control siRNA or 2 independent Spns2 siRNAs were detached, replated in collagen-coated 24-well plates (2.5×10^5 cells/well), and cultured for 12 hours. The cells were then washed twice with Medium 199 (Invitrogen) and incubated in 200 μl of Medium 199 containing 20 mM Hepes, pH 7.4, 10 mM sodium glycerophosphate, 5 mM sodium fluoride, 1 mM semicarbazide, 0.5% fatty acid free bovine serum albumin, 40 ng/ml vascular endothelial growth factor, 40 ng/ml fibroblast growth factor–2, and 400 ng/ml angiopoietin-1 for 12 hours. After incubation, conditioned medium was collected and centrifuged at 15,000 *g* for 5 minutes at 4°C to remove cell debris. S1P levels in the conditioned medium were determined as described below.

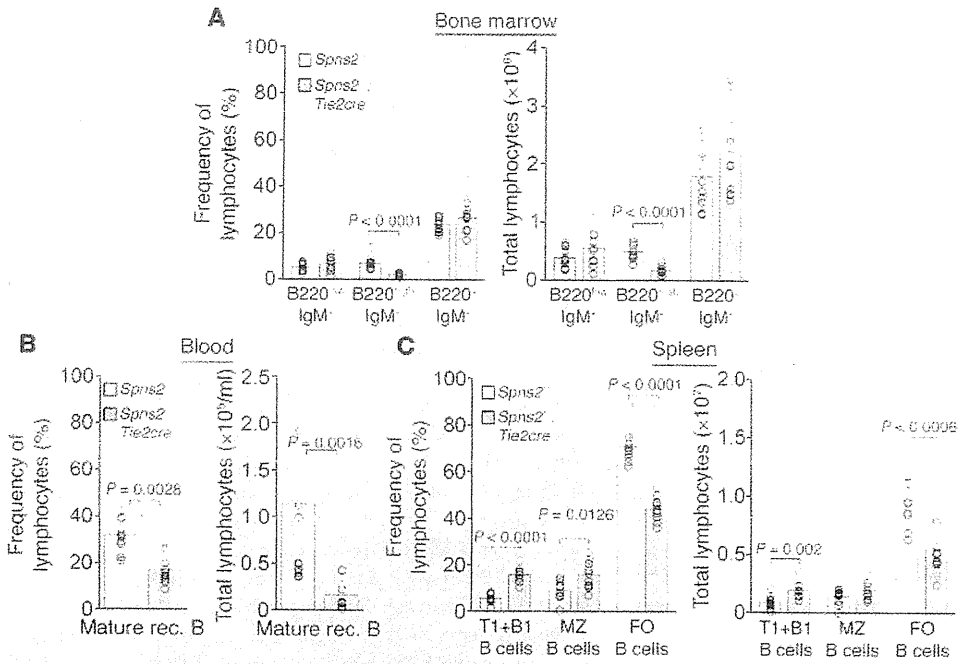

Figure 8

Spns2 expressed in ECs is required for immature B cell egress from bone marrow. (**A–C**) Flow cytometric analyses of lymphocytes of control (*Spns2$^{fl/fl}$*) or Spns2-ECKO (*Spns2$^{fl/fl}$;Tie2Cre*) mice. (**A**) Frequencies (left) and numbers (right) of pro–/pre–B cells (B220$^+$IgM$^-$), immature B cells (B220^{lo}IgM$^+$), and mature recirculating B cells (B220^{hi}IgM$^+$) in bone marrow are shown (n = 11). (**B**) Frequencies (left) and numbers (right) of mature recirculating B (Mature rec. B) cells (CD19$^+$CD23$^+$IgD$^+$) in peripheral blood are shown (n = 11). (**C**) Frequencies (left) and numbers (right) of T1 and B1 B cells (T1+B1), MZ, and follicular B cells in spleens are shown (n = 11). T1 and B1 B cells, MZ B cells, and follicular B cells were phenotypically defined as described in the legend of Figure 3D. In **A–C**, bars and circles indicate averages and values for individual mice, respectively.

Quantification of S1P using LC-MS/MS. Quantification of S1P was performed according to previously described methods (56) with minor modifications. Briefly, plasma and conditioned medium were mixed and sonicated with 10-fold volume of methanol and an internal standard (C17-S1P). Similarly, S1P extraction from cells was performed by homogenizing and sonicating cells in methanol. After centrifugation at 21,500 *g*, the resulting supernatant was recovered and used for the LC-MS/MS analysis. Then 20 μl of methanol extract was injected and separated by Nanospace LC (Shiseido) equipped with a C18 CAPCELL PAK ACR column (1.5 × 250 mm; Shiseido), using a gradient of solvent A (5 mM ammonium formate in water) and solvent B (5 mM ammonium formate in 95% [v/v] acetonitrile). Elution was sequentially ionized with an ESI probe, and the parent ion (m/z 380.2) and the fragment ion (m/z 264.2) were monitored in the positive mode by a Quantum Ultra Triple Quadrupole Mass Spectrometer (Thermo Fisher Scientific). Similarly, other lysophospholipids, including lysophosphatidic acid (LPA), lysophosphatidylcholine (LPC), lysophosphatidylethanolamine (LPE), lysophosphatidylglycerol (LPG), lysophosphatidylinositol (LPI), and lysophosphatidylserine (LPS), were extracted with methanol and analyzed by the LC-MS/MS system. For each lysophospholipid class, 12 acyl chains (14:0, 16:0, 16:1, 18:0, 18:1, 18:2, 18:3, 20:3, 20:4, 20:5, 22:5, and 22:6) were monitored.

For quantification of HDL- and albumin-bound S1P, mouse plasma was subjected to size-exclusion chromatography according to previously described methods (57) with some modifications. Briefly, 100 μl of plasma was loaded onto a Superose 12 column (GE Healthcare) using an ÄKTA Explorer System (GE Healthcare) and eluted with PBS at 0.25 ml/min at 4°C. Fractions were collected every 2 minutes (0.5 ml). S1P concentration in each fraction was determined by LC-MS/MS as described above.

Biochemical and hematological test of blood. Blood was collected from WT (*Spns2$^{+/+}$*, n = 4) and *Spns2$^{-/-}$* (*Spns2$^{-/-}$*, n = 4) mice via the abdominal aorta under inhalation anesthesia (isoflurane) using EDTA as an anticoagulant. Blood biochemistry parameters (total protein, total bilirubin, aspartate aminotransferase, alanine aminotransferase, triglycerol, glucose, blood urea nitrogen, and albumin) were determined by using a blood biochemical analyzer, Fuji DRI-CHEM 3500V (Fuji Film). Hematology and blood clotting parameters (white blood cells, red blood cells, platelets, hemoglobin, hematocrit, mean corpuscular volume, mean corpuscular hemoglobin, and mean corpuscular hemoglobin concentration) were determined by using an XT-1800iv hematology analyzer (Sysmex).

Antibodies and flow cytometric analysis. Unless otherwise stated, all anti-mouse monoclonal antibodies were obtained from eBiosciences Inc. Antibodies used for cell-surface staining were PE-conjugated anti-CD19 (ebio1D3), anti-CD8 (53-6.7), and anti-CD23 (B3B4); FITC-conjugated anti-B220 (RA3-6B2), anti-CD19 (1D3) (BD Biosciences), anti-CD8 (53-6.7) and anti-CD69 (H1.2F3) (BD Biosciences); APC-conjugated anti-CD62L (MEL-14) (BioLegend); Pacific Blue–conjugated anti-IgD (11-26) and anti-CD4 (RM4-5) (BD Biosciences); PeCy7-conjugated anti-IgM (II/41); and PerCP-Cy5.5 conjugated anti-CD21/CD35 (7E9) (BioLegend). Single-cell suspensions of freshly isolated thymus, spleen, peripheral lymph nodes (inguinal, axillary, and brachial), and total bone marrow cells of femur and tibia were subsequently incubated with anti-CD16/CD32 for 10 minutes, followed by staining with a combination of conjugated antibodies in FACS buffer (PBS + 4% heat-inactivated FCS + 2 mM EDTA) for 30 minutes. Before antibody staining, 250 μl of freshly isolated blood was treated with heparin solution, and red blood cells were lysed with BD Pharm Lyse solution (BD Biosciences) according to the manufacturer's protocol. Stained cells were analyzed on a FACSCanto II Flow Cytometer (BD Biosciences) equipped with blue (488 nm), violet (405 nm), and red (633 nm) lasers. FACS data were statistically analyzed with FlowJo software (TreeStar Inc.).

Histopathology and immunohistochemistry. Tissue samples from the spleen, thymus, axillary lymph nodes, mesenteric lymph nodes, and intestine (including Peyer patches) were collected from WT (*Spns2$^{+/+}$*, n = 3) and *Spns2$^{-/-}$* (*Spns2$^{-/-}$*, n = 3) mice and fixed in 20% neutral phosphate-buffered formalin. Each paraffin-embedded tissue was cut into 4-μm thickness and stained with H&E for light microscopy.

For immunohistochemistry, paraffin was then removed from the sections and antigen retrieval was performed in 10 mM citrate buffer (pH 6.0) by placing the sections in a pressure cooker for 3 minutes. Endogenous

peroxidase activity was blocked with 0.3% H_2O_2 in methanol. The sections were exposed to 1% BSA in PBS and were then incubated overnight at 4°C with goat anti-CD3ε (M-20; Santa Cruz Biotechnology Inc.). Immune complexes were labeled with biotinylated anti-goat IgG and streptavidin alkaline phosphatase (Nichirei). The signals were visualized with a Vector Blue Alkaline Phosphatase Substrate Kit (Vector Laboratories). For double immunostaining, sections were sequentially incubated with rat anti-CD45R (BD Biosciences — Pharmingen). Immune complexes were detected with HRP-conjugated anti-rat IgG (simple stain Max-Po; Nichirei) and 3-amino-9-ethyl carbazole (AEC) substrate system (Lab Vision) for color development.

S1P release from blood cells. Blood was collected from anesthetized WT (*Spns2*$^{+/+}$, $n = 4$) and *Spns2*$^{-/-}$ (*Spns2*$^{-/-}$, $n = 4$) mice via the inferior vena cava using heparinized syringes and transferred to tubes containing EDTA as an anticoagulant. Blood cells were separated from plasma by centrifugation at 1,200 *g* for 5 minutes at 4°C and washed twice with ice-cold PBS to remove plasma residues. The cells were resuspended in the ice-cold incubation buffer containing 20 mM Hepes, pH 7.4, 138 mM NaCl, 3.3 mM NaH_2PO_4, 2.9 mM KCl, 1.0 mM $MgCl_2$, 1 mg/ml glucose, and 1% fatty acid–free bovine serum albumin at a cell density of 5×10^8 cells/ml. Then 500 μl of blood cell suspensions (2.5×10^8 cells) was incubated at 4°C or at 37°C for 90 minutes. After incubation, the cells were pelleted by centrifugation at 1,200 *g* for 5 minutes at 4°C. The S1P levels in the supernatants were determined as described above. To quantify the total amount of S1P in the blood cells, cells were collected from 500 μl of cell suspensions by centrifugation at 1,200 *g* for 5 minutes at 4°C and homogenized in 100 μl of methanol.

Generation of bone marrow chimeras. Bone marrow chimeras were generated with 5×10^6 freshly isolated total bone marrow cells from femur and tibia of WT and Spns2 floxed mice (donor). Isolated cells were injected i.v. into lethally irradiated (900 cGY) *Spns2*$^{-/-}$ and Spns2-ECKO mice (host). Hematopoietic reconstitution of lymphoid organs of hosts by donor-derived cells was controlled 6 weeks after bone marrow transfer by genotyping of total bone marrow cells. Furthermore, lymphoid organs of reconstituted mice were FACS analyzed as described above.

In situ hybridization and immunohistochemistry on serial tissue sections. In situ hybridization and immunohistochemistry on serial tissue sections was performed by Genostaff. Briefly, the thymus, heart, lung, brain, and kidney of 8-week-old mice were dissected after perfusion, fixed with Tissue Fixative (Genostaff), and then embedded in paraffin by proprietary procedures and sectioned at 6 μm.

For in situ hybridization, tissue sections were de-waxed with xylene and rehydrated through an ethanol series and PBS. The sections were fixed with 4% paraformaldehyde in PBS for 15 minutes and then washed with PBS. The sections were treated with 8 μg/ml Proteinase K in PBS for 30 minutes at 37°C, washed with PBS, refixed with 4% paraformaldehyde in PBS, again washed with PBS, and placed in 0.2 N HCl for 10 minutes. After washing with PBS, the sections were acetylated by incubation in 0.1 M tri-ethanolamine-HCl, pH 8.0, 0.25% acetic anhydride for 10 minutes. After washing with PBS, the sections were dehydrated through a series of ethanol. The cDNA templates for Spns2 were 535-bp and 634-bp fragments corresponding to bases 1629–2163 and 2291–2924 of mouse Spns2 cDNA (GenBank NM_153060.2). Sense and antisense riboprobes for *Spns2* mRNA were synthesized using a digoxigenin RNA labeling kit (Roche) according to the manufacturer's protocol. Hybridization was performed with probes at concentrations of 300 ng/ml in the Probe Diluent-1 (Genostaff) at 60°C for 16 hours. After hybridization, the sections were washed in 5× HybriWash (Genostaff), equal to 5× SSC, at 50°C for 20 minutes and then in 50% formamide, 2× HybriWash at 50°C for 20 minutes, followed by RNase treatment in 50 μg/ml RNase A in 10 mM Tris-HCl, pH 8.0, 1 M NaCl, and 1 mM EDTA for 30 minutes at 37°C. Then the sections were washed twice with 2× HybriWash at 50°C for 20 minutes, twice with 2× HybriWash at 50°C for 20 minutes, and once with TBST (0.1% Tween 20 in TBS). After treatment with 0.5% blocking reagent (Roche) in TBST for 30 minutes, the sections were incubated with anti-DIG AP conjugate (Roche) diluted 1:1,000 with TBST for 2 hours at RT. The sections were washed twice with TBST and then incubated in 100 mM NaCl, 50 mM $MgCl_2$, 0.1% Tween 20, and 100 mM Tris-HCl, pH 9.5. Coloring reactions were performed with NBT/BCIP solution (Sigma-Aldrich) overnight and then washed with PBS. The sections were counterstained with Kernechtrot Stain Solution (Mutoh), dehydrated, and mounted with Malinol (DBS).

For immunohistochemistry, serial tissue sections were deparaffinized with xylene and rehydrated through an ethanol series and TBS. Endogenous peroxidase activity was blocked with 0.3% H_2O_2 in methanol for 30 minutes. For CD31 staining, the sections were treated with Protein Block (Dako) and avidin/biotin blocking kit (Vector), and incubated with 0.1 μg/ml of anti-CD31 rabbit polyclonal antibody (Spring Bioscience) at 4°C overnight. Immune complexes were labeled with biotin-conjugated goat anti-rabbit Ig (Dako) and peroxidase-conjugated streptavidin (Nichirei). For α-SMA staining, sections were treated with Blocking Reagent A (Nichirei) and incubated with anti–α-SMA mouse monoclonal antibody (Dako) at 4°C overnight. The sections were then blocked with Blocking Reagent B (Nichirei) and incubated with Simple Stain Mouse MAX-PO (M) (Nichirei). Peroxidase activity was visualized by diaminobenzidine. The sections were counterstained with Mayer's hematoxylin, dehydrated, and mounted with Malinol (Muto).

Statistics. Data were analyzed using GraphPad Prism software (GraphPad Software Inc.). Statistical significance was determined using a 2-tailed Mann-Whitney *U* test for paired samples or 1-way ANOVA and nonparametric tests for multiple groups. $P < 0.05$ was considered statistically significant.

Study approval. All animal experiments were approved by the animal committee of the National Cerebral and Cardiovascular Center and performed according to the regulations of the National Cerebral and Cardiovascular Center.

Acknowledgments

We thank T.N. Sato and M. Yanagisawa (Nara Institute of Science and Technology and University of Texas Southwestern Medical Center, respectively) for Tie2Cre mice. We are also grateful to K. Hiratomi, W. Koeda, M. Sone, H. Yonekawa, and Y. Matsuura for technical assistance, and to K. Shioya for providing excellent animal facilities. This work was supported in part by Grants-in-Aid for Scientific Research on Innovative Areas, "Fluorescence Live Imaging" (No. 22113009 to S. Fukuhara and No. 22113007 to M. Ishii) and "Neuro-Vascular Wiring" (No. 22122003 to N. Mochizuki), of The Ministry of Education, Culture, Sports, Science, and Technology, Japan; and by grants from the Japan Society for the Promotion of Science (to S. Fukuhara, M. Ishii, and N. Mochizuki); the Ministry of Health, Labour, and Welfare of Japan (to N. Mochizuki); the Program for the Promotion of Fundamental Studies in Health Sciences of the National Institute of Biomedical Innovation (to S. Fukuhara and N. Mochizuki); a grant from the International Human Frontier Science Program (to M. Ishii); the Takeda Science Foundation (to M. Ishii and N. Mochizuki); the Mitsubishi Foundation (to N. Mochizuki); the Japan Cardiovascular Research Foundation (to S. Fukuhara); and an AstraZeneca research grant (to N. Mochizuki).

Received for publication August 30, 2011, and accepted in revised form January 30, 2012.

Address correspondence to: Shigetomo Fukuhara or Naoki Mochizuki, Department of Cell Biology, National Cerebral and Cardiovascular Center Research Institute, 5-7-1 Fujishirodai, Suita, Osaka 565-8565, Japan. Phone: 81.6.6833.5012; Fax: 81.6.6835.5461; E-mail: fuku@ri.ncvc.go.jp (S. Fukuhara), nmochizu@ri.ncvc.go.jp (N. Mochizuki). Or to: Masaru Ishii, Laboratory of Cellular Dynamics, WPI-Immunology Frontier Research Center, Osaka University, 3-1 Yamada-oka, Suita, Osaka 565-0871, Japan. Phone: 81.6.6879.4268; Fax: 81.6.6879.8296; E-mail: mishii@ifrec.osaka-u.ac.jp.

1. Chi H. Sphingosine-1-phosphate and immune regulation: trafficking and beyond. *Trends Pharmacol Sci.* 2011;32(1):16–24.
2. Cyster JG. Chemokines, sphingosine-1-phosphate, and cell migration in secondary lymphoid organs. *Annu Rev Immunol.* 2005;23:127–159.
3. Hla T. Physiological and pathological actions of sphingosine 1-phosphate. *Semin Cell Dev Biol.* 2004; 15(5):513–520.
4. Rivera J, Proia RL, Olivera A. The alliance of sphingosine-1-phosphate and its receptors in immunity. *Nat Rev Immunol.* 2008;8(10):753–763.
5. Spiegel S, Milstien S. The outs and the ins of sphingosine-1-phosphate in immunity. *Nat Rev Immunol.* 2011;11(6):403–415.
6. Alvarez SE, et al. Sphingosine-1-phosphate is a missing cofactor for the E3 ubiquitin ligase TRAF2. *Nature.* 2010;465(7301):1084–1088.
7. Allende ML, Dreier JL, Mandala S, Proia RL. Expression of the sphingosine 1-phosphate receptor, S1P1, on T-cells controls thymic emigration. *J Biol Chem.* 2004;279(15):15396–15401.
8. Matloubian M, et al. Lymphocyte egress from thymus and peripheral lymphoid organs is dependent on S1P receptor 1. *Nature.* 2004;427(6972):355–360.
9. Pappu R, et al. Promotion of lymphocyte egress into blood and lymph by distinct sources of sphingosine-1-phosphate. *Science.* 2007;316(5822):295–298.
10. Schwab SR, Pereira JP, Matloubian M, Xu Y, Huang Y, Cyster JG. Lymphocyte sequestration through S1P lyase inhibition and disruption of S1P gradients. *Science.* 2005;309(5741):1735–1739.
11. Brinkmann V, et al. The immune modulator FTY720 targets sphingosine 1-phosphate receptors. *J Biol Chem.* 2002;277(24):21453–21457.
12. Graler MH, Goetzl EJ. The immunosuppressant FTY720 down-regulates sphingosine 1-phosphate G-protein-coupled receptors. *FASEB J.* 2004; 18(3):551–553.
13. Mandala S, et al. Alteration of lymphocyte trafficking by sphingosine-1-phosphate receptor agonists. *Science.* 2002;296(5566):346–349.
14. Brinkmann V, et al. Fingolimod (FTY720): discovery and development of an oral drug to treat multiple sclerosis. *Nat Rev Drug Discov.* 2010;9(11):883–897.
15. Allende ML, Tuymetova G, Lee BG, Bonifacino E, Wu YP, Proia RL. S1P1 receptor directs the release of immature B cells from bone marrow into blood. *J Exp Med.* 2010;207(5):1113–1124.
16. Pereira JP, Xu Y, Cyster JG. A role for S1P and S1P1 in immature-B cell egress from mouse bone marrow. *PLoS One.* 2010;5(2):e9277.
17. Schwab SR, Cyster JG. Finding a way out: lymphocyte egress from lymphoid organs. *Nat Immunol.* 2007; 8(12):1295–1301.
18. Breart B, et al. Lipid phosphate phosphatase 3 enables efficient thymic egress. *J Exp Med.* 2011; 208(6):1267–1278.
19. Zachariah MA, Cyster JG. Neural crest-derived pericytes promote egress of mature thymocytes at the corticomedullary junction. *Science.* 2010; 328(5982):1129–1135.
20. Pham TH, et al. Lymphatic endothelial cell sphingosine kinase activity is required for lymphocyte egress and lymphatic patterning. *J Exp Med.* 2010; 207(1):17–27.
21. Spiegel S, Milstien S. Functions of the multifaceted family of sphingosine kinases and some close relatives. *J Biol Chem.* 2007;282(4):2125–2129.
22. Kim RH, Takabe K, Milstien S, Spiegel S. Export and functions of sphingosine-1-phosphate. *Biochim Biophys Acta.* 2009;1791(7):692–696.
23. Hanel P, Andreani P, Graler MH. Erythrocytes store and release sphingosine 1-phosphate in blood. *FASEB J.* 2007;21(4):1202–1209.
24. Kobayashi N, et al. Sphingosine 1-phosphate is released from the cytosol of rat platelets in a carrier-mediated manner. *J Lipid Res.* 2006;47(3):614–621.
25. Yang L, Yatomi Y, Miura Y, Satoh K, Ozaki Y. Metabolism and functional effects of sphingolipids in blood cells. *Br J Haematol.* 1999;107(2):282–293.
26. Yatomi Y, et al. Sphingosine 1-phosphate, a bioactive sphingolipid abundantly stored in platelets, is a normal constituent of human plasma and serum. *J Biochem.* 1997;121(5):969–973.
27. Ito K, et al. Lack of sphingosine 1-phosphate-degrading enzymes in erythrocytes. *Biochem Biophys Res Commun.* 2007;357(1):212–217.
28. Olivera A, et al. The sphingosine kinase-sphingosine-1-phosphate axis is a determinant of mast cell function and anaphylaxis. *Immunity.* 2007; 26(3):287–297.
29. Kobayashi N, Kobayashi N, Yamaguchi A, Nishi T. Characterization of the ATP-dependent sphingosine 1-phosphate transporter in rat erythrocytes. *J Biol Chem.* 2009;284(32):21192–21200.
30. Mitra P, Oskeritzian CA, Payne SG, Beaven MA, Milstien S, Spiegel S. Role of ABCC1 in export of sphingosine-1-phosphate from mast cells. *Proc Natl Acad Sci U S A.* 2006;103(44):16394–16399.
31. Sato K, et al. Critical role of ABCA1 transporter in sphingosine 1-phosphate release from astrocytes. *J Neurochem.* 2007;103(6):2610–2619.
32. Takabe K, et al. Estradiol induces export of sphingosine 1-phosphate from breast cancer cells via ABCC1 and ABCG2. *J Biol Chem.* 2010; 285(14):10477–10486.
33. Kawahara A, Nishi T, Hisano Y, Fukui H, Yamaguchi A, Mochizuki N. The sphingolipid transporter spns2 functions in migration of zebrafish myocardial precursors. *Science.* 2009;323(5913):524–527.
34. Osborne N, et al. The spinster homolog, two of hearts, is required for sphingosine 1-phosphate signaling in zebrafish. *Curr Biol.* 2008; 18(23):1882–1888.
35. Campbell JJ, Pan J, Butcher EC. Cutting edge: developmental switches in chemokine responses during T cell maturation. *J Immunol.* 1999;163(5):2353–2357.
36. Weinreich MA, Hogquist KA. Thymic emigration: when and how T cells leave home. *J Immunol.* 2008;181(4):2265–2270.
37. Ge Q, Chen WF. Phenotypic identification of the subgroups of murine T-cell receptor alphabeta+ CD4+ CD8- thymocytes and its implication in the late stage of thymocyte development. *Immunology.* 1999;97(4):665–671.
38. Tian T, Zhang J, Gao L, Qian XP, Chen WF. Heterogeneity within medullary-type TCRαβ$^+$CD3$^+$CD4$^-$CD8$^+$ thymocytes in normal mouse thymus. *Int Immunol.* 2001;13(3):313–320.
39. Rosen H, Alfonso C, Surh CD, McHeyzer-Williams MG. Rapid induction of medullary thymocyte phenotypic maturation and egress inhibition by nanomolar sphingosine 1-phosphate receptor agonist. *Proc Natl Acad Sci U S A.* 2003; 100(19):10907–10912.
40. Argraves KM, Argraves WS. HDL serves as a S1P signaling platform mediating a multitude of cardiovascular effects. *J Lipid Res.* 2007;48(11):2325–2333.
41. Sato K, Okajima F. Role of sphingosine 1-phosphate in anti-atherogenic actions of high-density lipoprotein. *World J Biol Chem.* 2010;1(11):327–337.
42. Aoki S, et al. Sphingosine 1-phosphate-related metabolism in the blood vessel. *J Biochem.* 2005; 138(1):47–55.
43. Lee YM, Venkataraman K, Hwang SI, Han DK, Hla T. A novel method to quantify sphingosine 1-phosphate by immobilized metal affinity chromatography (IMAC). *Prostaglandins Other Lipid Mediat.* 2007;84(3–4):154–162.
44. Venkataraman K, et al. Vascular endothelium as a contributor of plasma sphingosine 1-phosphate. *Circ Res.* 2008;102(6):669–676.
45. Kisanuki YY, Hammer RE, Miyazaki J, Williams SC, Richardson JA, Yanagisawa M. Tie2-Cre transgenic mice: a new model for endothelial cell-lineage analysis in vivo. *Dev Biol.* 2001;230(2):230–242.
46. Schlaeger TM, et al. Uniform vascular-endothelial-cell-specific gene expression in both embryonic and adult transgenic mice. *Proc Natl Acad Sci U S A.* 1997; 94(7):3058–3063.
47. Takakura N, et al. A role for hematopoietic stem cells in promoting angiogenesis. *Cell.* 2000; 102(2):199–209.
48. Liu Y, et al. Edg-1, the G protein-coupled receptor for sphingosine-1-phosphate, is essential for vascular maturation. *J Clin Invest.* 2000;106(8):951–961.
49. Takada K, et al. Kruppel-like factor 2 is required for trafficking but not quiescence in postactivated T cells. *J Immunol.* 2011;186(2):775–783.
50. Nagasawa T. Microenvironmental niches in the bone marrow required for B-cell development. *Nat Rev Immunol.* 2006;6(2):107–116.
51. Osmond DG, Batten SJ. Genesis of B lymphocytes in the bone marrow: extravascular and intravascular localization of surface IgM-bearing cells in mouse bone marrow detected by electron-microscope radioautography after in vivo perfusion of 125I anti-IgM antibody. *Am J Anat.* 1984; 170(3):349–365.
52. Pereira JP, An J, Xu Y, Huang Y, Cyster JG. Cannabinoid receptor 2 mediates the retention of immature B cells in bone marrow sinusoids. *Nat Immunol.* 2009;10(4):403–411.
53. Yagi T, et al. A novel ES cell line, TT2, with high germline-differentiating potency. *Anal Biochem.* 1993; 214(1):70–76.
54. Zhang J, et al. Angiopoietin-1/Tie2 signal augments basal Notch signal controlling vascular quiescence by inducing delta-like 4 expression through AKT-mediated activation of beta-catenin. *J Biol Chem.* 2011;286(10):8055–8066.
55. Fukuhara S, et al. Differential function of Tie2 at cell-cell contacts and cell-substratum contacts regulated by angiopoietin-1. *Nat Cell Biol.* 2008; 10(5):513–526.
56. Inoue A, Arima N, Ishiguro J, Prestwich GD, Arai H, Aoki J. LPA-producing enzyme PA-PLA(1)alpha regulates hair follicle development by modulating EGFR signalling. *EMBO J.* 2011;19(16):4248–4260.
57. Tanaka M, Kishi Y, Takanezawa Y, Kakehi Y, Aoki J, Arai H. Prostatic acid phosphatase degrades lysophosphatidic acid in seminal plasma. *FEBS Lett.* 2004;571(1–3):197–204.

Intestinal CX_3C chemokine receptor 1^{high} (CX_3CR1^{high}) myeloid cells prevent T-cell-dependent colitis

Hisako Kayama[a,b,c], Yoshiyasu Ueda[a,b,c], Yukihisa Sawa[c,d,e], Seong Gyu Jeon[a,b,c], Ji Su Ma[a,b,c], Ryu Okumura[a,b,c], Atsuko Kubo[c,f], Masaru Ishii[c,f], Taku Okazaki[c,g], Masaaki Murakami[c,d,e], Masahiro Yamamoto[a,b,c], Hideo Yagita[h], and Kiyoshi Takeda[a,b,c,1]

[a]Laboratory of Immune Regulation, Department of Microbiology and Immunology, Graduate School of Medicine, Osaka University, Suita, Osaka, 565-0871, Japan; Laboratories of [b]Mucosal Immunology, [e]Developmental Immunology, and [f]Cellular Dynamics, World Premier International Research Center (WPI) Immunology Frontier Research Center, Osaka University, Suita, Osaka, 565-0871, Japan; [c]Core Research for Evolutional Science and Technology, Japan Science and Technology Agency, Saitama, 332-0012, Japan; [d]Laboratory of Developmental Immunology, Graduate School of Frontier Biosciences, Graduate School of Medicine, Osaka University, Suita, Osaka, 565-0871, Japan; [g]Division of Immune Regulation, Institute for Genome Research, University of Tokushima, Tokushima, 770-8503, Japan; and [h]Department of Immunology, Juntendo University School of Medicine, Tokyo, 113-8421, Japan

Edited by Warren Strober, National Institute of Allergy and Infectious Diseases, National Institutes of Health, Bethesda, MD, and accepted by the Editorial Board February 1, 2012 (received for review September 12, 2011)

Adequate activation of $CD4^+$ T lymphocytes is essential for host defense against invading pathogens; however, exaggerated activity of effector $CD4^+$ T cells induces tissue damage, leading to inflammatory disorders such as inflammatory bowel diseases. Several unique subsets of intestinal innate immune cells have been identified. However, the direct involvement of innate immune cell subsets in the suppression of T-cell-dependent intestinal inflammation is poorly understood. Here, we report that intestinal CX_3C chemokine receptor 1^{high} (CX_3CR1^{high}) $CD11b^+$ $CD11c^+$ cells are responsible for prevention of intestinal inflammation through inhibition of T-cell responses. These cells inhibit $CD4^+$ T-cell proliferation in a cell contact-dependent manner and prevent T-cell-dependent colitis. The suppressive activity is abrogated in the absence of the IL-10/Stat3 pathway. These cells inhibit T-cell proliferation by two steps. Initially, CX_3CR1^{high} $CD11b^+$ $CD11c^+$ cells preferentially interact with T cells through highly expressed intercellular adhesion molecule-1/vascular cell adhesion molecule-1; then, they fail to activate T cells because of defective expression of CD80/CD86. The IL-10/Stat3 pathway mediates the reduction of CD80/CD86 expression. Transfer of wild-type CX_3CR1^{high} $CD11b^+$ $CD11c^+$ cells prevents development of colitis in myeloid-specific Stat3-deficient mice. Thus, these cells are regulatory myeloid cells that are responsible for maintaining intestinal homeostasis.

mucosal immunology | innate immunity

Inflammatory bowel diseases (IBDs), represented by Crohn disease and ulcerative colitis in humans, result from genetic abnormalities, as well as uncontrolled intestinal immune responses toward commensal microflora and dietary antigens (1–3). Activation of appropriate mucosal immune responses is responsible for protection against pathogenic microorganisms, whereas excessive immune responses, especially unbalanced T-cell-mediated adaptive immune responses, to commensal microflora and dietary antigens lead to development of intestinal inflammation. Therefore, T-cell-mediated responses are tightly regulated to suppress aberrant inflammatory responses in the intestinal mucosa. Over the last few decades, $CD4^+$ regulatory T (T_{reg}) cells have been demonstrated to prevent T-cell-mediated chronic inflammatory diseases including IBDs (4, 5). Several possible mechanisms for this suppressive effect of T_{reg} cells have been proposed. Regulatory dendritic cells have also been implicated in the immune tolerance by inducing T_{reg} cells (6, 7). In tumor models, myeloid-derived suppressor cells (MDSCs) have been reported to suppress T-cell-mediated responses through several mechanisms (8, 9).

Several subsets of intestinal innate phagocytic cells have recently been identified that modulate intestinal homeostasis (10–12). In particular, $CD103^+$ CX_3CR1^- $CD11b^-$ dendritic cells (DCs) and CX_3CR1^+ $CD11b^+$ DCs have been well characterized (13–15). $CD103^+$ CX_3CR1^- $CD11b^-$ DCs have been shown to generate and activate gut-tropic $CD8^+$ T cells (16, 17). These DCs have further been shown to induce development of $Foxp3^+$ T_{reg} cells (18–20). CX_3CR1^+ $CD11b^+$ DCs have been shown to mediate inflammatory responses through the induction of Th1 and Th17 cell development (15, 21–24). In addition to these cell populations, $CD103^+$ CX_3CR1^- $CD11b^+$ cells and $CD11b^+CD11c^-$ macrophages have been identified in the intestinal lamina propria (13, 14, 22, 25). Other intestinal myeloid cell populations inducing T_{reg} cells have also been characterized (26–28). However, it remains unclear whether cell populations other than T_{reg} cells directly contribute to the suppression of inflammatory responses.

In this study, we characterized intestinal CX_3C chemokine receptor 1^{high} (CX_3CR1^{high}) $CD11b^+$ $CD11c^+$ cells, which show a cell contact-dependent suppression of T-cell proliferation, leading to prevention of intestinal inflammation.

Results

Intestinal CX_3CR1^{high} $CD11b^+$ $CD11c^+$ Cells Suppress T-Cell Growth. Several unique subsets of innate immune cells in the intestinal lamina propria have been identified (12–14, 16–26, 28–30). Among these subsets, $CD103^+$ CX_3CR1^- $CD11b^-$ $CD11c^+$ cells and CX_3CR1^+ $CD11b^+$ $CD11c^+$ cells have been reported to be major subsets in the intestine (13, 14). The functions of CX_3CR1^+ $CD11b^+$ $CD11c^+$ cells have been characterized in several aspects (13, 14, 17). However, the $CD11b^+$ $CD11c^+$ cell population could be divided into three subsets based on the expression level of CX_3CR1: CX_3CR1^{high}, $CX_3CR1^{intermediate\ (int)}$, and $CX_3CR1^{negative\ (-)}$ cells (Fig. S1A) (13, 17). Although previous studies have indicated the presence of CX_3CR1^{high} and CX_3CR1^{int} cells, differential functions of these cell subsets in T-cell differentiation have not been characterized (13, 17). Therefore, we examined the effects of three subsets on induction of Th1, Th17, and T_{reg} cells (Fig. 1A). CX_3CR1^{high}, CX_3CR1^{int}, and CX_3CR1^- cells were isolated from the colonic lamina propria and cultured with splenic naïve $CD4^+$ T cells for 4 d. $CD4^+$ T cells cocultured with CX_3CR1^{int} or CX_3CR1^- cells predominantly produced IL-17 or IFN-γ,

Author contributions: H.K. and K.T. designed research; H.K., Y.U., S.G.J., J.S.M., and R.O. performed research; Y.S., A.K., M.I., T.O., M.M., M.Y., and H.Y. contributed new reagents/analytic tools; H.K., Y.S., S.G.J., J.S.M., M.I., M.M., and K.T. analyzed data; and H.K. and K.T. wrote the paper.

The authors declare no conflict of interest.

This article is a PNAS Direct Submission. W.S. is a guest editor invited by the Editorial Board.

[1]To whom correspondence should be addressed. E-mail: ktakeda@ongene.med.osaka-u.ac.jp.

This article contains supporting information online at www.pnas.org/lookup/suppl/doi:10.1073/pnas.1114931109/-/DCSupplemental.

www.pnas.org/cgi/doi/10.1073/pnas.1114931109

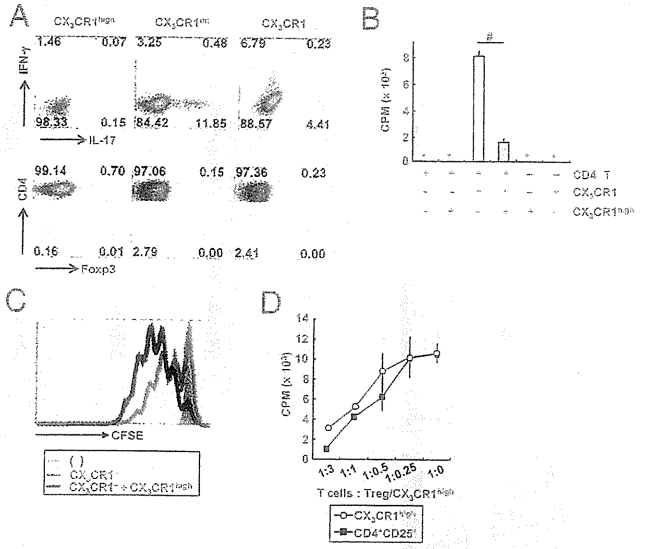

Fig. 1. CX_3CR1^{high} $CD11b^+$ $CD11c^+$ cells in the intestinal lamina propria suppress T-cell proliferation. (*A*) Flow cytometric plots of IL-17-, IFN-γ-, or Foxp3-expressing $CD4^+$ T cells cocultured with the indicated cells for 72 h. (*B*) [^{3}H]thymidine uptake of $CD4^+$ T cells cultured with the indicated cells. #$P <$ 0.022. (*C*) The fluorescence intensity of CFSE-labeled $CD4^+$ T cells cultured with the indicated cells at a ratio 1:1:1 for 72 h. (*D*) [^{3}H]thymidine uptake by $CD4^+$ T cells cocultured with CX_3CR1^- DCs in the presence of increasing ratios of splenic $CD4^+$ $CD25^+$ T_{reg} cells (closed rectangle) or colonic CX_3CR1^{high} cells (open circle). All data are representative of two independent experiments (means ± SD of duplicate well measurements).

respectively. In contrast, expression of IFN-γ, IL-17, or Foxp3 was not induced in $CD4^+$ T cells cocultured with the CX_3CR1^{high} cells. Next, we examined the effects on T-cell proliferation. $CD4^+$ T cells were cocultured with the CX_3CR1^{high}, CX_3CR1^{int}, or CX_3CR1^- cells for 72 h, and their proliferation was analyzed by assessing incorporation of [^{3}H]thymidine (Fig. S1*B*). $CD4^+$ T cells cocultured with CX_3CR1^- and CX_3CR1^{int} cells showed robust proliferative responses, indicating that the CX_3CR1^- and CX_3CR1^{int} cells had similar properties as DCs in enhancing T-cell responses. In contrast, $CD4^+$ T cells cocultured with CX_3CR1^{high} cells did not show any enhanced proliferation. These findings indicate that CX_3CR1^{high} cells are not typical DCs. Indeed, CX_3CR1^{high} cells express several macrophage-related molecules (CD14, CD68, and F4/80), as well as DC-related molecules (CD11c and DEC205) (Fig. S1*C*). In addition, CX_3CR1^{high} cells contain cytoplasmic vacuolar structures characteristic of macrophages (Fig. S1*D*) (14). We further found that the addition of CX_3CR1^{high} cells into a coculture of $CD4^+$ T cells and CX_3CR1^- DCs profoundly reduced T-cell proliferation (Fig. 1*B*). The suppression of T-cell proliferation by the CX_3CR1^{high} cells was further confirmed by reduced dilution of the fluorescence intensity of $CD4^+$ T cells labeled with carboxyfluorescein succinimidyl ester (CFSE) (Fig. 1*C*). We then compared the suppressive ability of CX_3CR1^{high} cells on T-cell proliferation with that of T_{reg} cells. $CD4^+$ T cells were cultured with DCs and anti-CD3 mAb in the presence of various numbers of T_{reg} cells or CX_3CR1^{high} cells (Fig. 1*D*). The CX_3CR1^{high} cells showed a dose-dependent suppression of T-cell proliferation in a very similar manner to that induced by T_{reg} cells. CX_3CR1^{high} cells isolated from $CX_3CR1^{+/GFP}$ mice, in which CX_3CR1 Ab staining was well correlated with GFP expression (Fig. S1*E*), also inhibited T-cell proliferation (Fig. S1*F*). CX_3CR1^{high} cells were not present in the $CD11b^+$ $CD11c^+$ population in the spleen, mesenteric lymph nodes (MLNs), or thymus (Fig. S1*G*). Collectively, our in vitro analyses suggested that a CX_3CR1^{high} $CD11b^+$ $CD11c^+$ subset of intestinal myeloid cells inhibited T-cell proliferation independently of T_{reg} induction.

CX_3CR1^{high} Myeloid Cells Prevent Intestinal Inflammation. We next assessed the in vivo function of the CX_3CR1^{high} subset of intestinal myeloid cells using a T-cell-dependent colitis model. Severe combined immunodeficiency (SCID) mice given $CD45RB^{high}$ $CD4^+$ T cells showed severe weight loss with severe intestinal pathology (Fig. 2 *A* and *B*). Cotransfer of CX_3CR1^{high} cells dramatically reduced their weight loss and the severity of intestinal inflammation. The cotransfer of CX_3CR1^{high} cells did not induce any change in the frequency of IL-17-, IFN-γ-, IL-4-, or IL-10-producing $CD4^+$ T cells or in the frequency of Foxp3-expressing $CD4^+$ T cells in the colonic lamina propria (Fig. S2). However, the total number of $CD4^+$ T cells in the lamina propria was markedly reduced by CX_3CR1^{high} cell coadministration (Fig. 2*C*). Assessment of CFSE dilution in transferred $CD45RB^{high}$ $CD4^+$ T cells demonstrated robust T-cell proliferation in the colonic lamina propria of *Rag2*$^{-/-}$ mice. However, cotransfer of CX_3CR1^{high} cells substantially inhibited CFSE dilution in transferred T cells (Fig. 2*D*). Transferred CX_3CR1^{high} cells were observed just beneath the epithelial cell layers of the intestine but

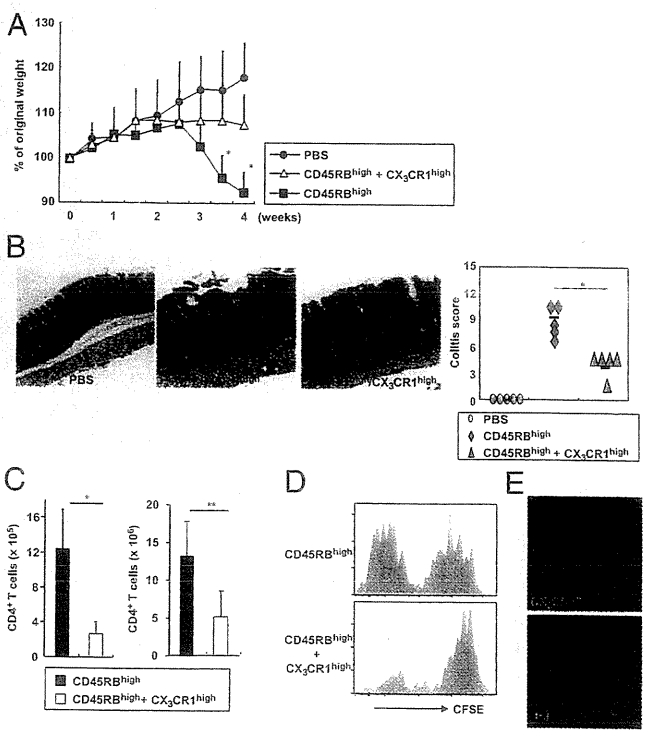

Fig. 2. CX_3CR1^{high} myeloid cells alleviate T-cell-dependent intestinal inflammation. (*A*) SCID mice were injected i.p. with 3×10^5 $CD45RB^{high}$ $CD4^+$ T cells or PBS (closed circles). After 2 h, 3×10^5 CX_3CR1^{high} cells were transferred (open triangles) or not (closed rectangles). Body weight change was monitored and is presented relative to initial body weight. *$P < 0.005$ ($n = 8$ per group). (*B*) Hematoxylin and eosin staining of colon sections at 4 wk after the transfer described in *A* (*Left*) and the colitis score (*Right*). *$P <$ 0.0012. (Original magnification, 200×.) (*C*) Numbers of large intestinal lamina propria $CD4^+$ T cells at 2 wk ($n = 4$ per group) (*Left*) and 4 wk ($n = 5$ per group) (*Right*) after transfer. *$P < 0.02$; **$P < 0.015$. (*D*) $CD45RB^{high}$ T cells (3×10^5) were labeled with CFSE and transferred into *Rag2*$^{-/-}$ mice with or without 3×10^5 CX_3CR1^{high} cells. After 12 d, CFSE dilution in colonic $CD4^+$ T cells was analyzed. (*E*) Cryosection of the colon from a SCID mouse at 3 d after i.v. injection of CFSE-labeled CX_3CR1^{high} cells. (Original magnification, 200×.) Data are representative of three independent experiments (*D* and *E*).

not in MLNs or spleen (Fig. 2*E* and Fig. S3 *A* and *B*). Transferred CX_3CR1^{high} cells were in close proximity to T cells in the lamina propria (Fig. S3*C*). In addition, the number of $CD4^+$ T cells was reduced where CX_3CR1^{high} cells were present (Fig. S3 *C* and *D*). Total number of CX_3CR1^{high} cells increased in the colonic lamina propria of the transferred mice (Fig. S4). Thus, the CX_3CR1^{high} subset of intestinal myeloid cells suppresses T-cell proliferation in the intestinal lamina propria, thereby preventing intestinal inflammation; hereafter, we call this subset CX_3CR1^{high} regulatory myeloid (M_{reg}) cells.

IL-10/Stat3-Dependent Suppressive Ability of CX_3CR1^{high} M_{reg} Cells. To determine how CX_3CR1^{high} M_{reg} cells exert their immunosuppressive function, we performed a comprehensive analysis of gene expression profiles in CX_3CR1^{high} M_{reg} cells. CX_3CR1^{high} M_{reg} cells expressed several IL-10-inducible genes such as *Hpgd*, *Cd163*, *Hmox1*, *Cd209f*, and *Cd209g* (Fig. S5*A*). Hence, we analyzed CX_3CR1^{high} M_{reg} cells in $Il10^{-/-}$ mice. Because normal numbers of CX_3CR1^{high} M_{reg} cells were observed in the colon of $Il10^{-/-}$ mice (Fig. S5*B*), we isolated these cells and analyzed the expression of the genes that were selectively expressed in wild-type CX_3CR1^{high} M_{reg} cells. Expression of *Hpgd*, *Cd163*, *Hmox1*, *Cd209f*, and *Cd209g* was severely decreased in $Il10^{-/-}$ cells despite normal expression of the myeloid cell-related gene *Cebpb* (Fig. 3*A*). CX_3CR1^{high} M_{reg} cells from LysM-*cre*; $Stat3^{fl/fl}$ mice ($Stat3^{-/-}$ CX_3CR1^{high} M_{reg} cells) also showed profoundly decreased levels of expression of these genes (Fig. 3*B*). To evaluate whether $Stat3^{-/-}$ CX_3CR1^{high} M_{reg} cells suppress the T-cell proliferative response, wild-type or $Stat3^{-/-}$ CX_3CR1^{high} M_{reg} cells were added to coculture of $CD4^+$ T cells with wild-type DCs (Fig. 3*C*). $Stat3^{-/-}$ CX_3CR1^{high} M_{reg} cells were not able to suppress T-cell proliferation. $Il10^{-/-}$ CX_3CR1^{high} M_{reg} cells were also defective in their suppression of T-cell proliferation (Fig. 4*E*). Furthermore, $Stat3^{-/-}$ CX_3CR1^{high} M_{reg} cells showed impaired prevention of intestinal inflammation in $Rag2^{-/-}$ mice given $CD45RB^{high}$ $CD4^+$ T cells (Fig. 3*D*). Thus, the suppressive function of CX_3CR1^{high} M_{reg} cells in vitro and in vivo was impaired in the absence of IL-10/Stat3 signaling.

CX_3CR1^{high} M_{reg} Cells Inhibit T-Cell Growth by Two Steps. We then assessed the mechanism underlying the suppression of T-cell proliferation by CX_3CR1^{high} M_{reg} cells. Because MDSCs have been reported to suppress T-cell response through arginase-1, inducible NOS, and reactive oxygen species (ROS) (8, 9), we analyzed the effects of inhibitors of these mediators. However, the inhibitors did not cancel the suppressive activity of CX_3CR1^{high} M_{reg} cells (Fig. S6 *A*–*E*). Expression of indoleamine 2, 3-dioxygenase (IDO) in several regulatory DCs inhibits T-cell responses (6, 20). However, T-cell proliferation was not increased by addition of an IDO inhibitor (Fig. S6*F*). Moreover, CX_3CR1^{high} M_{reg} cells did not express T_{reg}-related genes such as *Foxp3*, *Ctla4*, and *Folr4* (Fig. S6*G*). Thus, CX_3CR1^{high} M_{reg} cells possess distinct mechanisms from those used by those cells previously shown to inhibit T-cell proliferation. Coculture of CX_3CR1^{high} M_{reg} cells with $CD4^+$ T cells in transwell plates did not suppress T-cell proliferation, indicating that cell–cell contact is required for suppression (Fig. S6*H*). Addition of CX_3CR1^{high} M_{reg} cells to cocultures of $CD4^+$ T cells and DCs substantially decreased T-cell aggregation around DCs; instead, T cells preferentially associated with CX_3CR1^{high} M_{reg} cells (Fig. 4*A*). Inhibition of T-cell aggregation was not observed in $Stat3^{-/-}$ and $Il10^{-/-}$ CX_3CR1^{high} M_{reg} cells. Thus, CX_3CR1^{high} M_{reg} cells had a higher affinity to interact with T cells than DCs and, thereby, suppressed T-cell responses. These findings prompted us to investigate the expression of adhesion molecules that are involved in DC–T-cell interactions. Surface expression of intercellular adhesion molecule (ICAM)-1, ICAM-2, lymphocyte function-associated antigen (LFA)-1, and vascular cell adhesion molecule (VCAM)-1 was

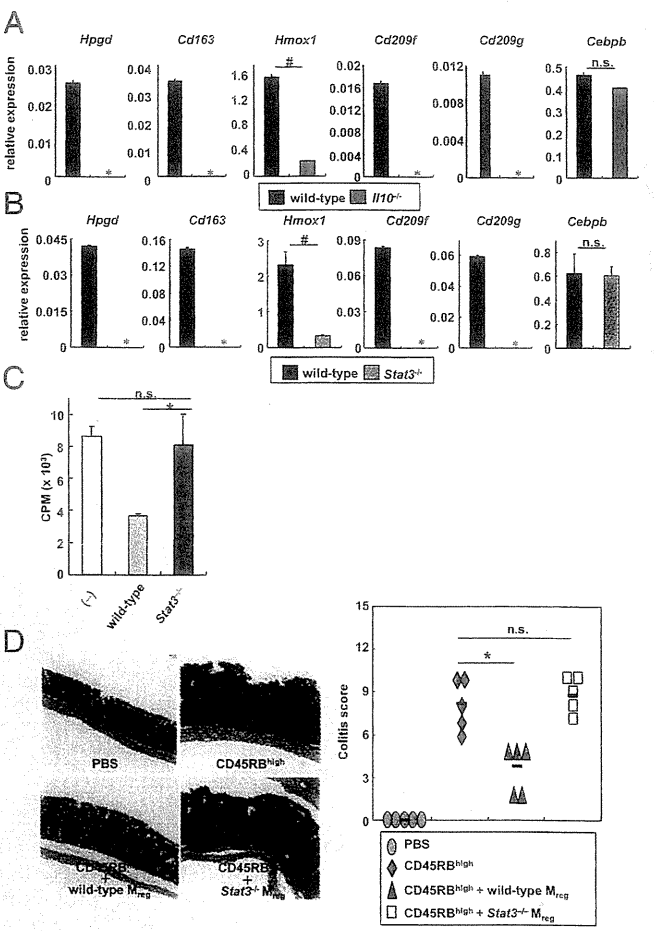

Fig. 3. Defective activity of $Stat3^{-/-}$ M_{reg} cells. (*A* and *B*) Expression of *Hpgd*, *Cd163*, *Hmox1*, *CD209f*, *CD209g*, and *Cebpb* mRNA in CX_3CR1^{high} M_{reg} cells from wild-type, $Il10^{-/-}$, and LysM-*cre*; $Stat3^{fl/fl}$ mice. Data are presentative of two independent experiments (means ± SD of at least triplicate PCRs on the identical sample). *, not detected; #$P < 0.025$. (*C*) [^{3}H]thymidine uptake by $CD4^+$ T cells cultured with CX_3CR1^- DCs in the presence of wild-type or $Stat3^{-/-}$ CX_3CR1^{high} M_{reg} cells. Data are representative of four independent experiments (means ± SD of triplicate well measurements). *$P < 0.047$. (*D*) Hematoxylin and eosin staining of colon sections of $Rag2^{-/-}$ mice given 3×10^5 $CD45RB^{high}$ $CD4^+$ T cells with 3×10^5 M_{reg} cells from wild-type or LysM-*cre*; $Stat3^{fl/fl}$ mice (*Left*) and colitis score (*Right*). (Original magnification, 200×.) *$P < 0.025$ ($n = 5$ per group).

considerably higher in CX_3CR1^{high} M_{reg} cells than in CX_3CR1^- DCs (Fig. 4*B*). Therefore, we analyzed whether these adhesion molecules are involved in the CX_3CR1^{high} M_{reg} suppressive activity. Treatment of CX_3CR1^{high} M_{reg} cells with blocking mAbs to ICAM-1, ICAM-2, LFA-1, and VCAM-1 canceled the CX_3CR1^{high} M_{reg} suppressive activity on T-cell proliferation (Fig. 4*C*). Treatment of CX_3CR1^{high} M_{reg} cells with each mAb did not abrogate the suppressive activity (Fig. S7*A*), but the combination of ICAM-1 and VCAM-1 mAbs substantially induced T-cell proliferation. In addition, treatment of CX_3CR1^{high} M_{reg} cells with mAbs to ICAM-1 and VCAM-1 resulted in increased aggregation of $CD4^+$ T cells around DCs (Fig. 4*D*). These results indicate that an ICAM-1/VCAM-1-mediated interaction is required for suppression. Expression of ICAM-1 and VCAM-1 was high in $Stat3^{-/-}$ and $Il10^{-/-}$ CX_3CR1^{high} M_{reg} cells, which showed impaired suppressive activity (Fig. 4*B* and Fig. S7*B*). In addition, T cells aggregated around $Stat3^{-/-}$ and $Il10^{-/-}$ CX_3CR1^{high} M_{reg} cells (Fig. 4*A*). Therefore, we analyzed how

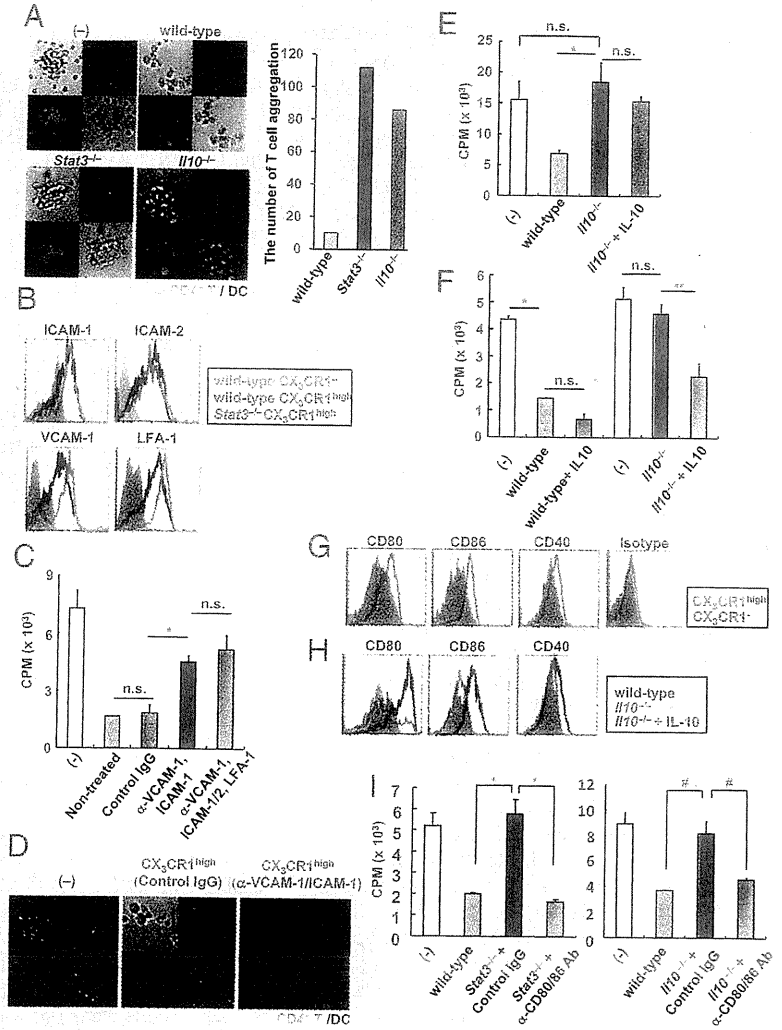

Fig. 4. Two-step mechanism for suppression of T-cell growth by M_{reg} cells. (*A*) Green dye-labeled $CD4^+$ T cells were cultured with nonlabeled CX_3CR1^- DCs and red dye-labeled M_{reg} cells from wild-type, LysM-*cre*; *Stat3*$^{fl/fl}$, or *Il10*$^{-/-}$ mice (*Left*). The number of T-cell aggregation in twenty fields (*Right*). (Original magnification, 100×.) (*B*) Expression of adhesion molecules on the indicated cells from wild-type and LysM-*cre*; *Stat3*$^{fl/fl}$ mice. (*C*) $CD4^+$ T cells and wild-type CX_3CR1^- DCs were cocultured with M_{reg} cells pretreated with the indicated blocking Abs or control Ig for evaluation of T-cell proliferation. $^*P < 0.012$. (*D*) Red dye-labeled CX_3CR1^{high} M_{reg} cells were treated with blocking Abs to ICAM-1 and VCAM-1 then added to the mixture of green dye-labeled $CD4^+$ T cells and nonstained CX_3CR1^- DCs. (Original magnification, 100×.) (*E*) IL-10 (100 ng/mL) was added to the coculture of $CD4^+$ T cells, wild-type DCs, and *Il10*$^{-/-}$ M_{reg} cells. Then, T-cell proliferation was measured. $^*P < 0.02$. (*F*) Wild-type and *Il10*$^{-/-}$ M_{reg} cells were preincubated with or without 100 ng/mL IL-10 for 72 h. Then, the cells were analyzed for the suppressive activity of T-cell proliferation. $^*P < 0.016$; $^{**}P < 0.034$. (*G*) Surface expression of CD80, CD86, CD40, and MHC class II on CX_3CR1^{high} M_{reg} cells and CX_3CR1^- DCs. (*H*) Expression of CD80, CD86, and CD40 on M_{reg} cells from wild-type and *Il10*$^{-/-}$ mice cultured for 48 h with or without 100 ng/mL IL-10. (*I*) *Stat3*$^{-/-}$ and *Il10*$^{-/-}$ M_{reg} cells were pretreated with the indicated blocking Abs. Then, M_{reg} cells were cultured with $CD4^+$ T cells and wild-type CX_3CR1^- DCs, and T-cell proliferation was measured. $^*P < 0.025$; $^\#P < 0.045$. All data are representative of at least two independent experiments (mean values ± SD of triplicate well measurements).

CX_3CR1^{high} M_{reg} cells with high affinity for T cells show IL-10-dependent suppression of T-cell proliferation. CX_3CR1^{high} M_{reg} cells produced IL-10 constitutively (Fig. S8 *A* and *B*). However, supplementation of exogenous IL-10 into cocultures of $CD4^+$ T cells and *Il10*$^{-/-}$ CX_3CR1^{high} M_{reg} cells did not induce the reduction of T-cell proliferative responses (Fig. 4*E*). In addition, the suppressive activity of wild-type CX_3CR1^{high} M_{reg} cells was not blocked in the presence of neutralizing Abs to IL-10 and the IL-10 receptor (Fig. S8*C*). Thus, IL-10 is not directly involved in the suppression of T-cell proliferation. However, IL-10 pretreatment of *Il10*$^{-/-}$, but not *Stat3*$^{-/-}$, CX_3CR1^{high} M_{reg} cells before coculture led to a substantial reduction of T-cell proliferative responses, indicating that IL-10 provides a key signal for CX_3CR1^{high} M_{reg} cells to acquire suppressive activity (Fig. 4*F* and Fig. S8*D*). Expression of molecules that transduce coinhibitory signals toward T cells, including B7-H4, herpesvirus entry mediator (HVEM), programmed death ligand (PD-L)1, and PD-L2 was increased in CX_3CR1^{high} M_{reg} cells compared with CX_3CR1^- DCs (Fig. S8*E*). However, expression of these coinhibitory molecules remained high in *Stat3*$^{-/-}$ CX_3CR1^{high} M_{reg} cells. Furthermore, the possible involvement of these inhibitory molecules in the suppressive activity of CX_3CR1^{high} M_{reg} cells was ruled out in experiments using neutralizing Abs and knockout mice (Fig. S8 *F*–*H*). In contrast, expression of CD80 and CD86 was severely decreased in CX_3CR1^{high} M_{reg} cells compared with that in CX_3CR1^- DCs, although MHC class II was equally and highly expressed in both populations (Fig. 4*G* and Fig. S8*C*). Notably, expression of CD80 and CD86 was considerably higher in *Il10*$^{-/-}$ and *Stat3*$^{-/-}$ CX_3CR1^{high} M_{reg} cells than in wild-type CX_3CR1^{high} M_{reg} cells (Fig. 4*H* and Fig. S9*A*). Furthermore, IL-10 treatment of *Il10*$^{-/-}$ CX_3CR1^{high} M_{reg} cells decreased the expression of CD80 and CD86 (Fig. 4*H*). Therefore, we suspected that CX_3CR1^{high} M_{reg} cells with decreased expression of costimulatory molecules compete with DCs to suppress T-cell proliferation. To test this, *Stat3*$^{-/-}$ and *Il10*$^{-/-}$ CX_3CR1^{high} M_{reg} cells were pretreated with blocking mAbs to CD80 and CD86, and then cocultured with $CD4^+$ T cells (Fig. 4*I*). *Stat3*$^{-/-}$ and *Il10*$^{-/-}$ CX_3CR1^{high} M_{reg} cells pretreated with mAbs to CD80 and CD86 suppressed T-cell proliferation. These findings clearly indicate that CX_3CR1^{high} M_{reg} cells suppress T-cell responses via a two-step mechanism: CX_3CR1^{high} M_{reg} cells interact with T cells with high affinity through high expression of adhesion molecules and then show IL-10-dependent suppression of CD80/CD86-mediated costimulatory signals, leading to inhibition of T-cell proliferation.

Defective CX_3CR1^{high} M_{reg} Function Results in Development of Colitis. The aberrant Th1/Th17-mediated responses attributable to enhanced DC activity have been considered to induce intestinal inflammation in *Il10*$^{-/-}$ mice and innate immune cell-specific Stat3 mutant mice (31–34). Because the function of CX_3CR1^{high} M_{reg} cells was impaired in the absence of IL-10/Stat3, we assessed

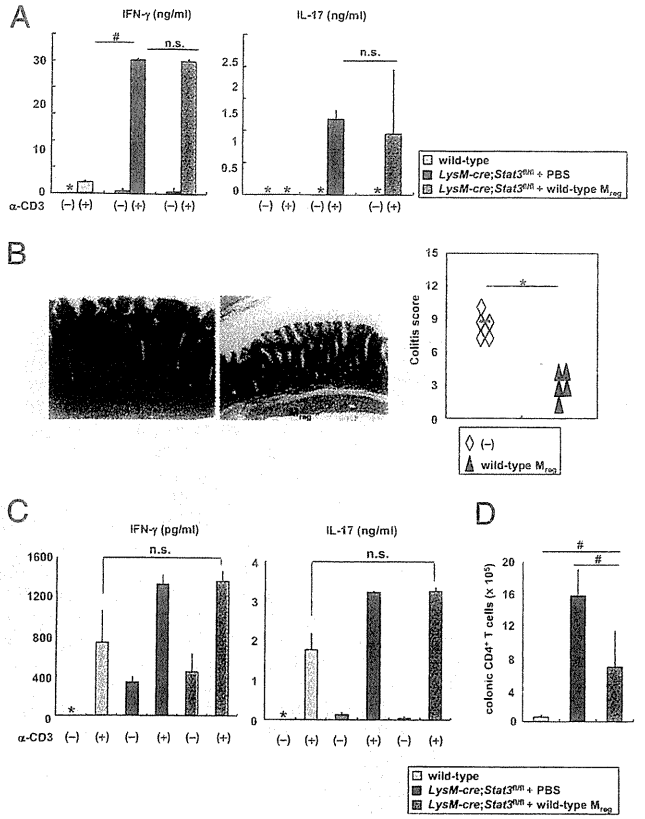

Fig. 5. Defective M_{reg} cell function leads to development of colitis. (*A*, *C*, and *D*) LysM-*cre*; *Stat3*$^{fl/fl}$ mice were transferred i.p. with 7×10^4 wild-type CX_3CR1^{high} M_{reg} cells at 4 and 6 wk of age. At 2 wk after the last transfer, splenic (*A*) or colonic lamina propria (*C*) $CD4^+$ T cells were analyzed for production of IFN-γ and IL-17A. *, not detected; $^{\#}P < 0.008$. Total number of $CD4^+$ T cells in the colonic lamina propria was analyzed (*D*). $^{\#}P < 0.0079$. Data are from two independent experiments with four mice per group. (*B*) Hematoxylin and eosin staining of colon sections at 2 wk after the last transfer (*Left*) and the colitis score (*Right*). (Original magnification, 200×.) $^*P < 0.0002$.

the involvement of CX_3CR1^{high} M_{reg} cells in the pathogenesis of intestinal inflammation in LysM-*cre*; *Stat3*$^{fl/fl}$ mice. LysM-*cre*; *Stat3*$^{fl/fl}$ mice were transferred with wild-type CX_3CR1^{high} M_{reg} cells and were analyzed for Th1 and Th17 activities. In LysM-*cre*; *Stat3*$^{fl/fl}$ mice, Th1 and Th17 activities, as determined by IFN-γ and IL-17A production from splenic $CD4^+$ T cells, respectively, were increased (Fig. 5*A*). Even in LysM-*cre*; *Stat3*$^{fl/fl}$ mice transferred with wild-type CX_3CR1^{high} M_{reg} cells, Th1 and Th17 activity remained considerably enhanced. However, the severity of intestinal inflammation was greatly improved in LysM-*cre*; *Stat3*$^{fl/fl}$ mice transferred with wild-type CX_3CR1^{high} M_{reg} cells (Fig. 5*B*). $CD4^+$ T cells in the colonic lamina propria produced increased amounts of IFN-γ and IL-17A even in LysM-*cre*; *Stat3*$^{fl/fl}$ mice transferred with wild-type CX_3CR1^{high} M_{reg} cells; however, the total number of $CD4^+$ T cells was markedly decreased in the lamina propria (Fig. 5 *C* and *D*). These findings demonstrate that the defective activity of CX_3CR1^{high} M_{reg} cells is critically involved in the development of spontaneous colitis when T cells are overactivated and that transfer of normal CX_3CR1^{high} M_{reg} cells is able to ameliorate the colitis.

Discussion

In the present study, we characterized the intestinal CX_3CR1^{high} $CD11b^+$ $CD11c^+$ M_{reg} cell subset, which directly inhibits T-cell proliferation and, thereby, prevents T-cell-dependent intestinal inflammation. The IL-10/Stat3 pathway is critically involved in the suppressive activity of CX_3CR1^{high} M_{reg} cells.

To date, $CD103^+$ CX_3CR1^- DCs and CX_3CR1^+ $CD11b^+$ $CD11c^+$ cells have been identified as major DC subsets in the intestine. Previous studies indicated that intestinal CX_3CR1^+ $CD11b^+$ $CD11c^+$ cells are further divided into two subsets based on the expression level of CX_3CR1, but these studies did not analyze differential functions of CX_3CR1^{high} and CX_3CR1^{int} cells (13, 17). This study clearly demonstrates that CX_3CR1^{high} $CD11b^+$ $CD11c^+$ cells are a regulatory myeloid cell subset possessing unique functions that directly suppress T-cell proliferation. Previous studies indicated that CX_3CR1^+ $CD11b^+$ $CD11c^+$ cells mediate inflammatory responses such as Th17 cell induction (21–23). In this regard, when splenic naïve $CD4^+$ T cells were cocultured with unsorted CX_3CR1^+ $CD11b^+$ $CD11c^+$ cells, including CX_3CR1^{high} and CX_3CR1^{int} cells, T cells did not vigorously proliferate, although they produced IL-17. In contrast, splenic naïve $CD4^+$ T cells cocultured with CX_3CR1^{int} subset robustly proliferated and produced higher amounts of IL-17 compared with T cells cocultured with unsorted CX_3CR1^+ $CD11b^+$ $CD11c^+$ cells (Fig. S9*B*). These observations would be attributable to suppression of T-cell proliferation by CX_3CR1^{high} M_{reg} cells present within the CX_3CR1^+ $CD11b^+$ $CD11c^+$ cell population. Thus, CX_3CR1^{high} and CX_3CR1^{int} cells are shown to possess distinct functions suppressing and activating T cells, respectively. At present, these functionally distinct populations can only be separated by expression level of CX_3CR1, indicating that both populations are related. It is possible that CX_3CR1^{int} cells are precursors of CX_3CR1^{high} cells, and both cell populations show plasticity. Several previous reports have shown that CX_3CR1^+ cells have macrophage-like properties (14, 15, 35, 36). Indeed, CX_3CR1^{high} M_{reg} cells show macrophage-like morphology and express macrophage-related surface markers. On the other hand, we found that *Stat3*$^{-/-}$ and *Il10*$^{-/-}$ CX_3CR1^{high} M_{reg} cells induced T-cell proliferation, indicating that CX_3CR1^{high} M_{reg} cells show DC-like properties in the absence of the IL-10/Stat3 signaling in vitro (Fig. S9*C*). Therefore, it is possible that CX_3CR1^{int} cells are precursors of CX_3CR1^{high} cells and terminally differentiate into CX_3CR1^{high} M_{reg} cells sharing some macrophage-like properties in response to IL-10.

Several regulatory subsets of myeloid cells, which might be related to M_{reg} cells, have been reported. Colonic IL-10-producing $F4/80^+$ $CD11b^+$ myeloid cells have been reported to mediate the maintenance of Foxp3 expression in T_{reg} cells (26). This subset is observed in MLNs, where M_{reg} cells are not present. Intestinal macrophages suppress T-cell responses via IL-10-dependent induction of T_{reg} cells (22). Unlike M_{reg} cells, these macrophages do not express CD11c, CD14, or DEC205. Most recently, the activity of intestinal macrophages has been shown to be regulated by CX_3CR1 (37). Indeed, mice deficient in CX_3CR1 were highly sensitive to intestinal inflammation induced by dextran sodium sulfate. These intestinal cells might include CX_3CR1^{high} M_{reg} cells. It is interesting to analyze the suppressive activity of CX_3CR1^{high} M_{reg} cells in CX_3CR1-deficient mice. MDSCs are also the cell population similar to CX_3CR1^{high} M_{reg} cells. However, MDSCs do not express CD11c or MHC class II and are hardly detected in healthy mice (9, 38), whereas CX_3CR1^{high} M_{reg} cells express CD11c and MHC class II and are abundant in the intestinal lamina propria of healthy mice. Expression of CX_3CR1^{high} M_{reg} cell-related genes (*Hpgd*, *Cd163*, *Hmox1*, *Cd209f*, and *Cd209g*) was severely reduced in MDSCs, whereas MDSC-related genes (*Arg1*, *Nos2*, *Cybb*, *S100a8*, and *S100a9*) were not expressed in CX_3CR1^{high} M_{reg} cells (Fig. S9 *D* and *E*).

$CD103^+$ CX_3CR1^- DCs have been shown to promote intestinal immune tolerance through the generation of $Foxp3^+$ T_{reg} cells (15, 16, 18, 19). Intestinal macrophages are also reported to induce $Foxp3^+$ T_{reg} cells (22). Intestinal epithelial cells have been implicated in promoting differentiation of $CD103^+$ DCs possessing

a property to induce T_{reg} cells (39, 40). CX_3CR1^{high} M_{reg} cells localize very close to intestinal epithelial cells. Therefore, intestinal epithelial cells might be involved in the final maturation (or differentiation) of CX_3CR1^{high} M_{reg} cells in the intestinal lamina propria through modulation of IL-10 production.

In the present study, we characterize intestinal CX_3CR1^{high} $CD11b^+$ $CD11c^+$ cells (CX_3CR1^{high} M_{reg} cells) that suppress intestinal inflammation through direct inhibition of T-cell proliferation in the intestinal lamina propria. T_{reg} cells with a normal suppressive activity are abundantly present in LysM-cre/$Stat3^{f/f}$ mice (33), indicating that defective activity of CX_3CR1^{high} M_{reg} cells can cause intestinal inflammation even in the presence of T_{reg} cells. Therefore, CX_3CR1^{high} M_{reg} cells maintain the intestinal homeostasis together with T_{reg} cells, as well as several innate cell subsets that have regulatory functions. Identification of an CX_3CR1^{high} M_{reg} population in the human intestines and characterization of human CX_3CR1^{high} M_{reg} function in patients with IBD will be a critical future issue in establishing their role in the pathogenesis of intestinal inflammation in humans.

Materials and Methods

Mice. C57BL/6J mice and BALB/c mice at 6–8 wk of age were purchased from CLEA Japan or Japan SLC. Male 6-wk-old CB17-SCID mice were purchased from CLEA Japan. LysM-*cre*; *Stat3*$^{fl/fl}$ mice and CX_3CR1-EGFP knock-in (heterozygous) mice were generated as described (32, 41, 42). *Il10*$^{-/-}$ mice were purchased from The Jackson Laboratory. Each mutant mouse strain was backcrossed onto a C57BL/6J background for at least five generations. All animal experiments were conducted in accordance with the guidelines of the Animal Care and Use Committee of Osaka University.

The details of reagents, isolation of lamina propria cells, histopathological score, and proliferation assay are described in *SI Materials and Methods*.

ACKNOWLEDGMENTS. We thank S. Sakaguchi and T. Hirano for fruitful discussions; C. Hidaka for secretarial assistance; E. Morii for histological analysis; J. Kikuta and E. Ohata for microscopy analysis; and K. Atarashi, D. Dodd, and Y. Magota for technical assistance. This work was supported by a grant-in-aid from the Ministry of Education, Culture, Sports, Science and Technology; the Ministry of Health, Labour and Welfare; The Kato Memorial Trust for Nambyo Research; the Osaka Foundation for the Promotion of Clinical Immunology; and the Takeda Science Foundation.

1. Bouma G, Strober W (2003) The immunological and genetic basis of inflammatory bowel disease. *Nat Rev Immunol* 3:521–533.
2. Xavier RJ, Podolsky DK (2007) Unravelling the pathogenesis of inflammatory bowel disease. *Nature* 448:427–434.
3. Strober W, Fuss I, Mannon P (2007) The fundamental basis of inflammatory bowel disease. *J Clin Invest* 117:514–521.
4. Wing K, Sakaguchi S (2010) Regulatory T cells exert checks and balances on self tolerance and autoimmunity. *Nat Immunol* 11:7–13.
5. Sakaguchi S, Wing K, Onishi Y, Prieto-Martin P, Yamaguchi T (2009) Regulatory T cells: How do they suppress immune responses? *Int Immunol* 21:1105–1111.
6. Morelli AE, Thomson AW (2007) Tolerogenic dendritic cells and the quest for transplant tolerance. *Nat Rev Immunol* 7:610–621.
7. Wakkach A, et al. (2003) Characterization of dendritic cells that induce tolerance and T regulatory 1 cell differentiation in vivo. *Immunity* 18:605–617.
8. Gabrilovich DI, Nagaraj S (2009) Myeloid-derived suppressor cells as regulators of the immune system. *Nat Rev Immunol* 9:162–174.
9. Ostrand-Rosenberg S, Sinha P (2009) Myeloid-derived suppressor cells: Linking inflammation and cancer. *J Immunol* 182:4499–4506.
10. Laffont S, Powrie F (2009) Immunology: Dendritic-cell genealogy. *Nature* 462: 732–733.
11. Strober W (2009) The multifaceted influence of the mucosal microflora on mucosal dendritic cell responses. *Immunity* 31:377–388.
12. Coombes JL, Powrie F (2008) Dendritic cells in intestinal immune regulation. *Nat Rev Immunol* 8:435–446.
13. Varol C, et al. (2009) Intestinal lamina propria dendritic cell subsets have different origin and functions. *Immunity* 31:502–512.
14. Bogunovic M, et al. (2009) Origin of the lamina propria dendritic cell network. *Immunity* 31:513–525.
15. Niess JH, Adler G (2010) Enteric flora expands gut lamina propria CX3CR1+ dendritic cells supporting inflammatory immune responses under normal and inflammatory conditions. *J Immunol* 184:2026–2037.
16. Johansson-Lindbom B, et al. (2005) Functional specialization of gut CD103+ dendritic cells in the regulation of tissue-selective T cell homing. *J Exp Med* 202:1063–1073.
17. Schulz O, et al. (2009) Intestinal CD103+, but not CX3CR1+, antigen sampling cells migrate in lymph and serve classical dendritic cell functions. *J Exp Med* 206: 3101–3114.
18. Coombes JL, et al. (2007) A functionally specialized population of mucosal CD103+ DCs induces Foxp3+ regulatory T cells via a TGF-beta and retinoic acid-dependent mechanism. *J Exp Med* 204:1757–1764.
19. Sun CM, et al. (2007) Small intestine lamina propria dendritic cells promote de novo generation of Foxp3 T reg cells via retinoic acid. *J Exp Med* 204:1775–1785.
20. Matteoli G, et al. (2010) Gut CD103+ dendritic cells express indoleamine 2,3-dioxygenase which influences T regulatory/T effector cell balance and oral tolerance induction. *Gut* 59:595–604.
21. Uematsu S, et al. (2008) Regulation of humoral and cellular gut immunity by lamina propria dendritic cells expressing Toll-like receptor 5. *Nat Immunol* 9:769–776.
22. Denning TL, Wang YC, Patel SR, Williams IR, Pulendran B (2007) Lamina propria macrophages and dendritic cells differentially induce regulatory and interleukin 17-producing T cell responses. *Nat Immunol* 8:1086–1094.
23. Atarashi K, et al. (2008) ATP drives lamina propria T(H)17 cell differentiation. *Nature* 455:808–812.
24. Manocha M, et al. (2009) Blocking CD27-CD70 costimulatory pathway suppresses experimental colitis. *J Immunol* 183:270–276.
25. Ueda Y, et al. (2010) Commensal microbiota induce LPS hyporesponsiveness in colonic macrophages via the production of IL-10. *Int Immunol* 22:953–962.
26. Murai M, et al. (2009) Interleukin 10 acts on regulatory T cells to maintain expression of the transcription factor Foxp3 and suppressive function in mice with colitis. *Nat Immunol* 10:1178–1184.
27. Manicassamy S, et al. (2010) Activation of beta-catenin in dendritic cells regulates immunity versus tolerance in the intestine. *Science* 329:849–853.
28. Siddiqui KR, Laffont S, Powrie F (2010) E-cadherin marks a subset of inflammatory dendritic cells that promote T cell-mediated colitis. *Immunity* 32:557–567.
29. Takada Y, et al. (2010) Monocyte chemoattractant protein-1 contributes to gut homeostasis and intestinal inflammation by composition of IL-10-producing regulatory macrophage subset. *J Immunol* 184:2671–2676.
30. Jung S (2010) Dendritic cells: A question of upbringing. *Immunity* 32:502–504.
31. Kühn R, Löhler J, Rennick D, Rajewsky K, Müller W (1993) Interleukin-10-deficient mice develop chronic enterocolitis. *Cell* 75:263–274.
32. Takeda K, et al. (1999) Enhanced Th1 activity and development of chronic enterocolitis in mice devoid of Stat3 in macrophages and neutrophils. *Immunity* 10:39–49.
33. Kobayashi M, et al. (2003) Toll-like receptor-dependent production of IL-12p40 causes chronic enterocolitis in myeloid cell-specific Stat3-deficient mice. *J Clin Invest* 111: 1297–1308.
34. Melillo JA, et al. (2010) Dendritic cell (DC)-specific targeting reveals Stat3 as a negative regulator of DC function. *J Immunol* 184:2638–2645.
35. Niess JH (2010) What are CX3CR1+ mononuclear cells in the intestinal mucosa? *Gut Microbes* 1:396–400.
36. Scott CL, Aumeunier AM, Mowat AM (2011) Intestinal CD103+ dendritic cells: Master regulators of tolerance? *Trends Immunol* 32:412–419.
37. Medina-Contreras O, et al. (2011) CX3CR1 regulates intestinal macrophage homeostasis, bacterial translocation, and colitogenic Th17 responses in mice. *J Clin Invest* 121:4787–4795.
38. Youn JI, Nagaraj S, Collazo M, Gabrilovich DI (2008) Subsets of myeloid-derived suppressor cells in tumor-bearing mice. *J Immunol* 181:5791–5802.
39. Iliev ID, Mileti E, Matteoli G, Chieppa M, Rescigno M (2009) Intestinal epithelial cells promote colitis-protective regulatory T-cell differentiation through dendritic cell conditioning. *Mucosal Immunol* 2:340–350.
40. Iliev ID, et al. (2009) Human intestinal epithelial cells promote the differentiation of tolerogenic dendritic cells. *Gut* 58:1481–1489.
41. Ishii M, et al. (2009) Sphingosine-1-phosphate mobilizes osteoclast precursors and regulates bone homeostasis. *Nature* 458:524–528.
42. Jung S, et al. (2000) Analysis of fractalkine receptor CX(3)CR1 function by targeted deletion and green fluorescent protein reporter gene insertion. *Mol Cell Biol* 20: 4106–4114.